BAMS Article

Accomplishments of NOAA's Airborne Hurricane Field Program and a Broader Future Approach to Forecast Improvement

Jonathan Zawislak, Robert F. Rogers, Sim D. Aberson, Ghassan J. Alaka Jr., George R. Alvey III, Altug Aksoy, Lisa Bucci, Joseph Cione, Neal Dorst, Jason Dunion, Michael Fischer, John Gamache, Sundararaman Gopalakrishnan, Andrew Hazelton, Heather M. Holbach, John Kaplan, Hua Leighton, Frank Marks, Shirley T. Murillo, Paul Reasor, Kelly Ryan, Kathryn Sellwood, Jason A. Sippel, and Jun A. Zhang

ABSTRACT: Since 2005, NOAA has conducted the annual Intensity Forecasting Experiment (IFEX), led by scientists from the Hurricane Research Division at NOAA's Atlantic Oceanographic and Meteorological Laboratory. They partner with NOAA's Aircraft Operations Center, who maintain and operate the WP-3D and Gulfstream IV-SP (G-IV) Hurricane Hunter aircraft, and NCEP's National Hurricane Center and Environmental Modeling Center, who task airborne missions to gather data used by forecasters for analysis and forecasting and for ingest into operational numerical weather prediction models. The goal of IFEX is to improve tropical cyclone (TC) forecasts using an integrated approach of analyzing observations from aircraft, initializing and evaluating forecast models with those observations, and developing new airborne instrumentation and observing strategies targeted at filling observing gaps and maximizing the data's impact in model forecasts. This summary article not only highlights recent IFEX contributions toward improved TC understanding and prediction, but also reflects more broadly on the accomplishments of the program during the 16 years of its existence. It describes how IFEX addresses high-priority forecast challenges, summarizes recent collaborations, describes advancements in observing systems monitoring structure and intensity, as well as in assimilation of aircraft data into operational models, and emphasizes key advances in understanding of TC processes, particularly those that lead to rapid intensification. The article concludes by laying the foundation for the next generation of IFEX as it broadens its scope to all TC hazards, particularly rainfall, storm-surge inundation, and tornadoes, that have gained notoriety during the last few years after several devastating landfalling TCs.

KEYWORDS: Hurricanes/typhoons; Tropical cyclones; Aircraft observations; Model evaluation/performance; Model initialization; Field experiments

https://doi.org/10.1175/BAMS-D-20-0174.1

Corresponding author: Jonathan Zawislak, jonathan.zawislak@noaa.gov

In final form 14 May 2021

AFFILIATIONS: **Zawislak, Alvey, Aksoy, Dunion, Fischer, Hazelton, Leighton, Ryan, Sellwood, and Zhang**—National Oceanographic and Atmospheric Administration/Atlantic Oceanographic and Meteorological Laboratory/Hurricane Research Division, and Cooperative Institute for Marine and Atmospheric Studies, University of Miami, Miami, Florida; **Rogers, Aberson, Alaka, Bucci, Cione, Dorst, Gamache, Gopalakrishnan, Kaplan, Marks, Murillo, Reasor, and Sippel**—National Oceanographic and Atmospheric Administration/Atlantic Oceanographic and Meteorological Laboratory/Hurricane Research Division, Miami, Florida; **Holbach**—National Oceanographic and Atmospheric Administration/Atlantic Oceanographic and Meteorological Laboratory/Hurricane Research Division, Miami, and Northern Gulf Institute, Florida State University, Tallahassee, Florida

During the past five years, the United States has experienced multiple tropical cyclone (TC) landfalls that caused over a billion dollars in damage [National Centers for Environmental Information (NCEI); NCEI 2020]: Hurricanes Matthew (2016), Harvey (2017), Irma (2017), Maria (2017), Florence (2018), Michael (2018), Dorian (2019), Isaias (2020), Laura (2020), Sally (2020), and Tropical Storm Imelda (2019). In 2020 alone, 12 named storms made landfall in the United States, 6 of which were hurricanes, during a record-breaking North Atlantic hurricane season.

Many of these TCs made landfall as major hurricanes (categories 3–5 on the Saffir–Simpson hurricane wind scale, or maximum sustained surface wind speed > 95 kt; 1 kt ≈ 0.5 m s^{-1}). Storm-surge inundation, extreme rainfall, high surf, and tornadoes (Table 1) were significant contributors to the damage, in addition to high winds; in fact, flooding from rainfall and surge accounts for the majority of deaths in landfalling storms (Rappaport 2000). A common feature among most of these TCs is that they underwent at least one period of rapid intensification (RI), typically defined as an intensity increase of 30 kt or more in 24 h (Kaplan and DeMaria 2003).

Although improvements in intensity forecast skill have lagged improvements in track forecasts over the last 30 years, there has been a notable decrease in intensity forecast errors and improved model skill over the past 10 years (Cangialosi et al. 2020). That said, forecasters continue to struggle to predict the onset and magnitude of RI, a challenge that is one of the high-priority objectives of the Weather Research and Forecasting Innovation Act of 2017[1] and NOAA's Hurricane Forecast Improvement Project (HFIP; Gall et al. 2013; Marks et al. 2019).

[1] www.congress.gov/bill/115th-congress/house-bill/353/

Improving TC forecasts requires advancements in multiple areas, including developing new observing technologies and strategies that fill existing temporal and spatial gaps in observing networks, improving the assimilation of those observations into numerical models, and improving the models themselves, for instance through the use of observations to evaluate and improve how well a model simulates a TC. Although satellites are one of the primary platforms to observe TC characteristics (Rogers et al. 2019) and improve model initialization through assimilation (e.g., Goerss 2009; Christophersen et al. 2018; Magnusson et al. 2019), aircraft continue to be a necessary platform for obtaining in situ measurements at a spatial resolution adequate enough to resolve structures within the inner core.

In 2005, the Hurricane Research Division (HRD) at NOAA's Atlantic Oceanographic and Meteorological Laboratory (AOML) began their Intensity Forecasting Experiment (IFEX), a program dedicated toward using existing airborne tools with new observing strategies, numerical models, and data assimilation to improve intensity prediction. Three primary IFEX goals were defined as follows (Rogers et al. 2006, hereafter R06): 1) collect observations that span the TC life cycle in a variety of environments for model initialization and evaluation; 2) develop and refine measurement strategies and technologies that provide

Table 1. A summary of the hazards experienced during recent landfalling TCs. Landfall locations are provided for each storm, as well as the peak rainfall measured, observed or estimated maximum storm-surge inundations, the best track maximum sustained wind speed at landfall, and the number of tornadoes observed in the United States. All information is taken from NHC tropical cyclone reports. In "rainfall," boldface text indicates > 20 in., while in "wind" boldface text indicates major hurricane landfalls and italic text further indicates a category 5.

Storm (year)	Landfall location	Rainfall (in.)	Surge inundation (ft)	Wind (kt)	U.S. tornadoes
Matthew (2016; Stewart 2017)	Haiti	**23.80**	Unknown	**130**	2
	Cuba	**26.40**	13	**115**	
	Bahamas	19.70	8	**115**	
	South Carolina	18.95	7.7	75	
Harvey (2017; Blake and Zelinsky 2018)	Barbados	Unknown	Unknown	40	52
	Saint Vincent	Unknown	Unknown	40	
	Texas[a]	**60.58**	10	**115**	
Irma (2017; Cangialosi et al. 2018)	Barbuda	Unknown	8	***155***	25
	Saint Martin	Unknown	Unknown	***155***	
	British Virgin Islands	Unknown	Unknown	***155***	
	Bahamas	Unknown	Unknown	**135**	
	Cuba	**23.90**	10	***145***	
	Florida Keys	6–10	8	**115**	
	Florida	**21.66**	10	**100**	
Maria (2017; Pasch et al. 2019)	Dominica	**22.80**	Unknown	***145***	3[b]
	Puerto Rico	**37.90**	9	**135**	
Florence (2018; Stewart and Berg 2019)	North Carolina	**35.93**	11	80	44
Michael (2018; Beven et al. 2019)	Florida	11.45	14	***140***	16
Dorian (2019; Avila et al. 2020)	Barbados	Unknown	Unknown	45	21
	Saint Lucia	Unknown	Unknown	45	
	Saint Croix	Unknown	Unknown	65	
	Saint Thomas	Unknown	Unknown	70	
	Bahamas[c]	**22.84**	20[d]	***160***	
	North Carolina	15.21	7	85	
Imelda (2019; Latto and Berg 2020)	Texas	**44.29**	2	40	2
Isaias (2020; Latto et al. 2021)	Dominican Republic	8	Unknown	55	39
	Bahamas	Unknown	Unknown	70	
	North Carolina	9.15	6	80	
Laura (2020; Pasch et al. 2021)	Louisiana[e]	11.74	18	**130**	16
Sally (2020; Berg and Reinhart 2021)	Alabama[f]	**29.99**	7	95	16

[a] Only the first U.S. landfall is shown. A second landfall occurred 4 days later near Cameron, Louisiana.

[b] In Puerto Rico, unconfirmed by the National Weather Service.

[c] Only the first Bahamas landfall at Elbow Cay is shown. A second landfall occurred 9 h later at Grand Bahama.

[d] Eyewitness account, but not an official measurement.

[e] Only the landfall in Louisiana is shown here, but Laura also made landfall as a tropical storm in Antigua, Nevis, the Dominican Republic, and Cuba.

[f] Only the hurricane landfall is shown here; Sally also made landfall near Cutler Bay, Florida, as a 30-kt TD on 12 Sep.

improved real-time monitoring of TC intensity, structure, and environment; and 3) improve the understanding of physical processes important for intensity change for a TC at all stages of its life cycle.

IFEX operates as a partnership between AOML/HRD; NOAA's Office of Marine and Aviation Operations (OMAO) Aircraft Operations Center (AOC), who maintain and operate two Lockheed WP-3D Orion (P-3) turboprops and the Gulfstream IV-SP (G-IV) jet; the 53rd U.S. Air Force Reserve Weather Reconnaissance Squadron (53rd WRS), who also fly TC missions;

NOAA/NCEP National Hurricane Center (NHC), who establish the priorities and needs that motivate IFEX; and NOAA/NCEP Environmental Modeling Center (EMC), who develop and implement the operational models, notably the Hurricane Weather Research and Forecasting (HWRF) Model.

IFEX also partners with HFIP, which was established in 2007 in response to the active and devastating 2004 and 2005 hurricane seasons (Gall et al. 2013; Gopalakrishnan et al. 2020). HFIP contributes to TC forecast improvement though the development of numerical weather prediction models, e.g., HWRF, the "basin-scale" version of HWRF (HWRF-B; Zhang et al. 2016; Alaka et al. 2017, 2019), and the next-generation Hurricane Analysis and Forecast System (HAFS) (Dong et al. 2020; Hazelton et al. 2020). HFIP invests in forecast improvements not only through advancements of existing models and development of new models, but also in the techniques by which they assimilate observations, and the postprocessing, production, and visualization of model products. Given the observational needs for both data assimilation and model evaluation, HFIP benefits from IFEX data collection.

The goal of this article is not only to highlight IFEX activities since the previous summaries (R06; Rogers et al. 2013a, hereafter R13), but to reflect on IFEX accomplishments after 16 years of existence, including how the program contributes to improving TC intensity forecasts through basic research and transition of that research into operations. This summary article serves as a culmination of IFEX by reviewing the program's invaluable contributions to understanding and predicting TCs. It will conclude with the path forward, introducing the next generation of NOAA's airborne hurricane field program as it evolves and broadens to meet the future needs of the TC forecasting community, and how it will contribute in a new era of HFIP.

Summary of IFEX missions

The primary crewed aircraft used by NOAA for hurricane reconnaissance, surveillance, and research, are the two P-3s and the G-IV. IFEX uses both types of aircraft to sample a variety of spatial and temporal scales (R13). The P-3s primarily sample the structure of the TC inner core (within 200 km of the center) during about a 3–4-h period at altitudes typically around 1.5–10 kft (1 kft ≈ 0.3 km), while the G-IV flies at a much higher altitude (41–45 kft) in the near environment (~150–300 km from the center) to the outer environment (>300 km) around the TC.

While the NOAA aircraft are flown for dedicated IFEX research missions, IFEX also benefits from data collection from other missions flown for operational NHC and EMC taskings by integrating research opportunities into those operational missions. For this reason, contributions from all NOAA aircraft missions are considered in IFEX-related studies, regardless of whether or not the missions were "dedicated" to research data collection.

NHC-tasked P-3 reconnaissance missions primarily focus on providing real-time guidance on the TC's intensity (10-m maximum sustained wind speed) and minimum sea level pressure (MSLP), center location, and the radial extent of 34-, 50-, and 64-kt winds; information that contributes to the "TCVitals" dataset, which is one of the inputs for initialization of models. Data gathered from those missions are also used subjectively by NHC to adjust their official intensity forecasts. NHC-tasked G-IV synoptic surveillance missions release dropsondes in the environment around TCs to help initialize models and are especially targeted at synoptic flow features that have the potential to interact with a TC during its life cycle and impact a storm's track forecast (Aberson 2003, 2010). EMC-tasked missions will be described in the next section.

Table 2 lists some of the notable TCs flown by NOAA since R13. NOAA aircraft sampled all U.S. landfalling hurricanes between 2016 and 2020 in addition to other impactful TCs such as Hurricane Joaquin (2015), a poorly forecasted storm that rapidly intensified unexpectedly and took 33 lives in the sinking of the *El Faro* (Berg 2016), and Hurricane Lorenzo (2020),

Table 2. List of notable pre-TC, tropical storms (TS), and hurricanes (HU) flown by NOAA aircraft in the Atlantic, east Pacific (EP), and central Pacific (CP) since 2013 and the last IFEX summary (R13), including the takeoff dates of NOAA flights, NOAA aircraft involved, the number of missions by each airplane (N42 and N43 are the P-3s, and N49 is the G-IV), number of dropsondes released by NOAA aircraft, number of tail Doppler radar analyses currently available, and commentary on why these storms are notable. Storms may be notable for unique instrumentation flown [e.g., Doppler wind lidar (DWL) and small uncrewed aircraft systems (sUAS)] and/or collaborations with NESDIS, Hurricane and Severe Storm Sentinel (HS3), Tropical Cyclone Intensity (TCI), Tropical Cyclone Rapid Intensification (TCRI), Sensing Hazards with Operational Unmanned Technology (SHOUT), and Organization of Tropical East Pacific Convection (OTREC), all described further in the sidebar on "Field program collaborations."

Storm	Dates of NOAA missions	NOAA aircraft	NOAA dropsondes	Number of radar analyses	Comments
TS Gabrielle	31 Aug–10 Sep 2013	N42 (1), N43 (2), N49 (2)	86	0	Genesis research, collaborative with HS3
HU Cristobal	23–27 Aug 2014	N42 (3), N43 (5), N49 (2)	168	24	Collaborative with HS3 and NESDIS Ocean Winds
HU Edouard	11–19 Sep 2014	N42 (3), N43 (6), N49 (1)	120	13	High density of ocean measurements; Coyote sUAS; collaborative with HS3 and NESDIS Ocean Winds during RI
TS Erika	25–28 Aug 2015	N43 (5), N49 (3)	155	19	Saharan Air Layer Experiment; sampled with DWL; collaborative with HS3 and TCI; RI null case
HU Joaquin	29 Sep–2 Oct 2015	N49 (5)	145	0	Collaborative with TCI
HU Patricia (EP)	21–23 Aug 2015	N43 (3)	29	6	Collaborative with TCI and NESDIS Ocean Winds; sampling during RI
HU Earl	2–3 Aug 2016	N43 (3)	34	8	Sampled with DWL on P-3
HU Hermine	25 Aug–1 Sep 2016	N43 (11)	116	46	Collaborative with SHOUT; sampled pre-RI and during RI, landfall
HU Matthew	29 Sep–8 Oct 2016	N43 (9), N49 (8)	349	21	Collaborative with SHOUT and NESDIS Ocean Winds; sampled during RI
TS Javier (EP)	8–9 Aug 2016	N43 (2)	17	5	Sampled with DWL on P-3; Coyote sUAS
HU Harvey	22–25 Aug 2017	N42 (4), N49 (4)	171	8	Sampled during RI
HU Irma	3–9 Sep 2017	N42 (8), N49 (8)	325	25	Sampled during RI and eyewall replacement cycles
HU Maria	19–26 Sep 2017	N42 (8), N49 (4)	210	28	Sampled with DWL; Coyote sUAS
HU Nate	5–10 Oct 2017	N42 (5), N49 (4)	187	12	Sampled with DWL; sampled RI event with ocean measurements
HU Lane (EP/CP)	19–22 Aug 2018	N42 (4), N49 (4)	189	13	Sampled with DWL; sampled RI; first central Pacific storm flown by NOAA P-3
Pre-Sergio (EP)	26–28 Sep 2018	N42 (3)	50	13	Genesis research flown from Costa Rica
HU Florence	8–13 Sep 2018	N42 (3), N49 (9)	368	10	Collaborative with NESDIS Ocean Winds; sampled RI
HU Michael	8–10 Oct 2018	N42 (6), N49 (3)	193	16	Sampled RI with extensive ocean measurements; Coyote sUAS
Pre-Ivo (EP)	17–20 Aug 2019	N42 (4)	67	14	Collaborative sampling with OTREC during genesis
HU Dorian	25 Aug–5 Sep 2019	N42 (15), N49 (10)	624	70	Sampled RI; collaborative with NESDIS Ocean Winds
HU Lorenzo	27–29 Sep 2019	N42 (1), N43 (2), N49 (3)	120	10	Sampled RI; collaborative with NESDIS Ocean Winds
HU Laura	20–26 Aug 2020	N42 (6), N43 (5) N49 (6)	407	38	Sampled RI
HU Sally	13–15 Sep 2020	N42 (1), N43 (3), N49 (3)	226	18	Sampled RI; collaborative with ONR TCRI
HU Teddy	15–22 Sep 2020	N42 (3), N43 (2), N49 (3)	98	22	Collaborative with ONR TCRI, NESDIS Ocean Winds, Stanford University
HU Delta	5–9 Oct 2020	N42 (4), N43 (4) N49 (4)	345	39	Sampled RI; collaborative with ONR TCRI

which despite never making landfall had 19 direct fatalities (11 in the sinking of the tug supply vessel *Bourbon Rhode*, and eight drownings due to rip currents generated on the East Coast of the United States; Zelinsky 2019).

Other TCs were notable for collaborative sampling conducted by IFEX with aircraft from other agencies (see sidebar on "Field program collaborations"). IFEX benefits most when it collaborates with coinciding NOAA field experiments and those of other agencies (such as NASA, ONR, and NSF/NCAR), which bring additional airborne and instrument assets into the field. These collaborative opportunities offer additional temporal, spatial, and vertical sampling with instruments that complement and fill observing gaps that exist within the typical NOAA instrument payloads. An example is shown in Fig. 1 where the P-3 and NASA Global Hawk (GH) flew collaborative missions in Hurricane Edouard in 2014.

Since the beginning of IFEX, there have been a total of 728 NOAA research and operational missions (P-3s and G-IV combined) into 122 TCs and pre-TCs. Of those, 268 sampled in and around tropical storms (TS), 218 missions in category-1 and category-2 hurricanes, and 165 missions in major hurricanes (Fig. 2a). The 2020 season made a large contribution to these numbers as it set records for NOAA and 53rd WRS hurricane flight operations—86 total NOAA missions were flown between the P-3s and G-IV (Table 3), and over 220 missions flown between NOAA and 53rd WRS combined.

The relative lack of flights into the formative (pre-TCs) and early stages [defined as TS, tropical depression (TD)] in the pre-IFEX years (Table 3) had been emphasized as an observing gap at the start of IFEX. As Table 3 and Fig. 2a show, filling this gap during IFEX has been a partial success as TS flights have represented the largest percentage of missions flown in the life cycle—especially in 2020 where half of the NOAA flights were in the TS stage. Flights into the formative stage,

Field program collaborations

IFEX continues to partner with the NOAA/NESDIS/Center for Satellite Application and Research (STAR) Ocean Winds program, which uses P-3 instrumentation—notably the Imaging Wind and Rain Airborne Profiler (IWRAP) (Fernandez et al. 2005; Guimond et al. 2014)—in hurricanes and winter storms to calibrate and validate satellite-borne remote sensors that measure the ocean surface-wind field and to explore new technologies for future satellites.

From 2012 to 2014, IFEX partnered with NASA's Hurricane and Severe Storm Sentinel (HS3; Braun et al. 2016). The goal of HS3 was to understand the relative roles of inner-core and environmental processes in the formation and intensification of TCs. HS3 used two Global Hawks (GHs), uncrewed aircraft capable of long duration sampling (up to 24 h) at high altitudes (55–65 kft). The biggest success of this collaboration was the sampling of Hurricane Edouard (2014) with coinciding GH, P-3, and G-IV flights (Fig. 1), as well as Coyote sUAS released from the P-3 (Cione et al. 2016). IFEX subsequently partnered with NOAA's Sensing Hazards with Operational Unmanned Technology (SHOUT) in 2015–16, a program that used the GH to evaluate how observations from high-altitude UAS improve TC forecasts and other high-impact weather (Wick et al. 2020). IFEX-SHOUT flew several collaborative missions into Hermine, Karl, and Matthew, which optimized sampling of the TC inner core and surrounding environment.

IFEX also partnered with the ONR Tropical Cyclone Intensity Experiment (TCI) in 2015, whose primary goal was to explore the TC upper-level outflow layer and its relationship to rapid changes in TC intensity and structure (Doyle et al. 2017). TCI used the NASA's high-altitude WB-57 aircraft, along with a High-Definition Sounding System (Black et al. 2017) on board, capable of deploying dropsondes at a relatively high sampling rate (e.g., dozens of dropsondes launched at ~20-s intervals). Successful collaborations between IFEX and TCI were carried out during three consecutive days into Hurricane Patricia (21–23 October 2015). During this period, observations from the WB-57 and P-3 documented a period of extreme RI when Patricia's maximum sustained wind speed increased by 105 kt in just 24 h (minimum central pressure decrease of 95 hPa), the most rapid intensification on record (Rogers et al. 2017). Beginning in 2020, IFEX began collaborating with ONR once again for their Departmental Research Initiative (DRI) Tropical Cyclone Rapid Intensification (TCRI) program, which leverages NOAA aircraft data to better understand and predict RI. Highlights from TCRI 2020 included high-density dropsonde observations during RI in Sally and Delta (Table 2)

In 2019, IFEX partnered with the NSF/NCAR Organization of Tropical East Pacific Convection (OTREC) experiment (Fuchs-Stone et al. 2020). The objective of OTREC was to use measurements from the NCAR/NSF G-V, along with enhanced radiosonde coverage in the region, to determine how the large-scale environment modulates the characteristics of deep convection in the southwest Caribbean and eastern North Pacific. OTREC and IFEX flew a 5-day series of missions from Costa Rica into the disturbance that eventually developed into Tropical Storm Ivo.

however, have been far fewer with only 30 TD and 47 pre-TC (i.e., pregenesis) missions in the IFEX period. And since 2015, the percentage of missions flown at this stage decreased from the first 10 years of IFEX (Table 3). This decrease reflects the opportunities that different seasons offer within the aircraft operating range and the tasking requirements for the aircraft. A considerable proportion of flights since 2015 have been dedicated to flying operational taskings in TCs threatening landfall, and many of those were already at hurricane strength by the first mission.

Figure 2b shows the rates of intensity change experienced by TCs 24 h after a given P-3 or G-IV mission, if the storm persists. Only a slight majority of flights were flown in strengthening TCs (>5 kt in 24 h; 241 flights), with a nearly equal amount of flights (226) flown in TCs that subsequently weakened (<–5 kt in 24 h) or remained steady state (–5 to 5 kt in 24 h). As RI is a priority for IFEX, it is notable that 63 missions were flown in TCs that subsequently rapidly intensified (≥30 kt in 24 h), most of which were in TSs and category-1 hurricanes (Fig. 2a). Also of note are the 57 missions into rapidly weakening (≤–30 kt in 24 h) events, many of those weakening due to landfall.

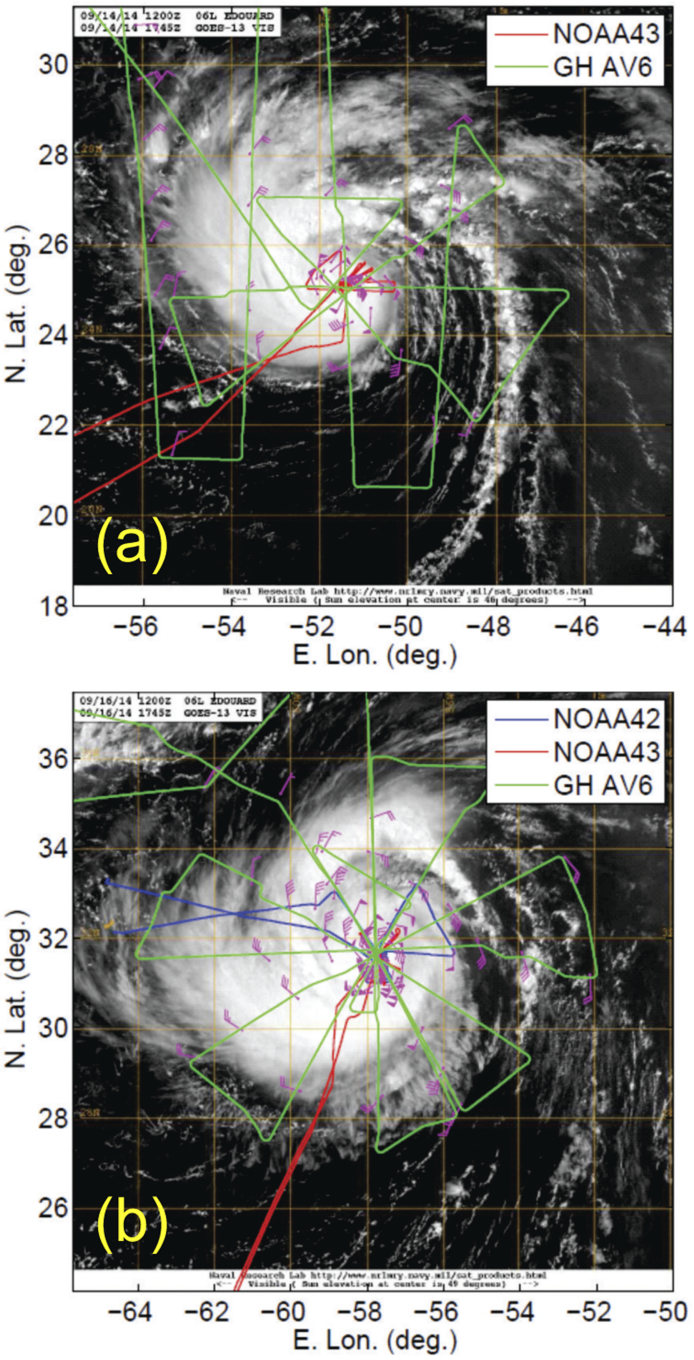

Fig. 1. Storm-relative flight tracks for the P-3s ("NOAA42," blue, and "NOAA43," red) and NASA Global Hawk ("GH AV6," green) into Hurricane Edouard on (a) 14 Sep 2014 (when the storm was intensifying) and (b) 16 Sep 2014 (storm was steady state) and near-surface winds from dropsondes (wind barbs) overlaid over visible satellite imagery. Figure is adapted from Rogers et al. (2016).

IFEX goal 1: Collect observations that span the TC life cycle in a variety of environments for model initialization and evaluation

Model initialization. IFEX data have been used in three ways in model initialization to improve TC forecasts: 1) by assimilation into operational numerical forecast models; 2) through research focused on improving how these data are assimilated into those models; and 3) design of new observing strategies to optimize collection of those data and model impacts.

Data assimilation advances in operational HWRF. EMC assimilates a suite of aircraft reconnaissance data from the NOAA aircraft and the 53rd WRS into its models.[2] HWRF in particular assimilates all available flight-level, dropsonde, and surface wind speed observations from the Stepped Frequency Microwave Radiometer (SFMR). In addition, the P-3s are tasked by

[2] While the global models (e.g., GFS and ECMWF) assimilate some reconnaissance data, the focus here will be on the impact of reconnaissance data in HWRF, which accepts nearly the complete suite of real-time reconnaissance data.

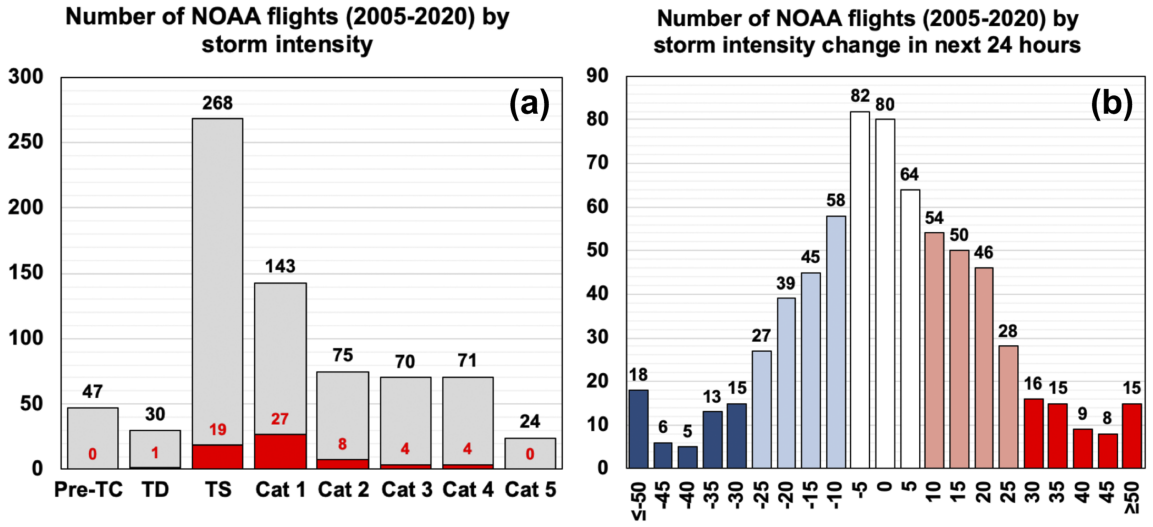

Fig. 2. Number of NOAA flights (includes both the G-IV and P-3s) for the IFEX period (2005–20) categorized by (a) storm intensity spanning the storm life cycle, including the pregenesis ("pre-TC") period, with the number of RI flights at those intensities indicated in red; and (b) intensity change (kt) 24 h after the mission, with intensification highlighted in red (rapid intensification in dark red), weakening in blue (rapid weakening in dark blue), and steady state in white. Storm intensity is defined as the best track maximum wind speed representative during the mission, while the change is defined by the difference between the best track intensity 24 h later and the representative intensity during the mission.

EMC and NHC to provide data from the tail Doppler radar (TDR), an instrument unique to the NOAA aircraft that retrieves 3D Doppler velocity and reflectivity in precipitation. Taskings are governed through close coordination between EMC, NHC, and HRD for potential landfall threats to the United States.

The groundwork for P-3 TDR missions was established around 2010 when advancements in the assimilation of TDR Doppler velocity data using the experimental Penn State University (PSU) data assimilation system resulted in lower track and intensity errors than those from operational NWP at the time (Zhang et al. 2011; Weng and Zhang 2012). These results were later expanded and confirmed using HRD's Hurricane Experimental Data Assimilation System (HEDAS; Aksoy et al. 2012, 2013; Aberson et al. 2015). Given these successes, real-time transmission and assimilation of TDR data became an operational priority. The real-time data were first assimilated into the operational HWRF during Tropical Storm Karen (2013), where it substantially reduced positive biases in intensity forecasts (Tong et al. 2014).

Despite these and other studies (e.g., Aberson et al. 2015; Weng and Zhang 2016) that showed benefits from assimilating the full suite of reconnaissance data, impacts were

Table 3. Number of NOAA flights flown in pre-IFEX years, during IFEX in 5-yr increments (2005–09, 2010–14, and 2015–19), and in 2020, and in subsequent rows, the percentage of the total flights for each period flown across various intensities in the storm life cycle. The representative intensity for each flight is defined from the best track. The "pre-IFEX" percentages are taken from Table 2 in R06.

	Pre-IFEX	IFEX 2005–09	IFEX 2010–14	IFEX 2015–19	IFEX 2020
Number of flights		230	180	232	86
Pre-TC (%)	4.3	6.5	10.0	5.6	0.0
TD (%)	7.2	5.2	3.4	3.9	3.5
TS (%)	26.8	37.0	36.1	33.6	47.7
Categories 1–2 (%)	31.6	27.4	41.1	22.0	34.9
Categories 3–5 (%)	30.0	23.9	9.4	34.9	13.9

somewhat mixed in early versions of the operational HWRF (Tong et al. 2018). Though the data did improve forecasts for TSs, they degraded hurricane forecasts due to inadequacies in the HWRF data assimilation system and large biases in the model physics.

In response to these inadequacies, since 2013 HWRF has made notable advances in both model physics (Zhang et al. 2015, 2017b, 2018a; Wang et al. 2018) and data assimilation (Pu et al. 2016; Lu et al. 2017; Winterbottom et al. 2018; Tong et al. 2018; Zhang et al. 2018; Zhang et al. 2020), enabling expanded use of reconnaissance data and resulting in a noticeable improvement in the track (Fig. 3a) and intensity (Fig. 3b) forecast skill of HWRF. With system improvements HWRF now makes better use of available data as it assimilates all NOAA and 53rd WRS reconnaissance data transmitted in real time. The result is that, between 2015 and 2019, HWRF was the most accurate TC intensity model in the Atlantic for the 48-h lead time that NHC uses for watch issuances (Cangialosi et al. 2020).

Benefits from improvements in model physics and data assimilation were further realized when EMC assessed the impact of reconnaissance data in a 2019 version of HWRF for all high-impact TCs in the Atlantic basin from 2016 to 2018. They found that including reconnaissance data improves the intensity forecast by 10%–15% through the 72-h lead time (Fig. 4). This represents a substantial improvement considering that this sample is dominated by many forecast cycles with major hurricanes, for which the impact of reconnaissance was negative in Tong et al. (2018). Recent testing suggests that the positive impact of reconnaissance data in HWRF has further increased since 2019 (HWRF Implementation Team 2021, personal correspondence), and continued advancements are expected as data assimilation and model physics further improve.

Data assimilation advancements through research and development. Developed at HRD as a unique data assimilation research tool, HEDAS produces high-resolution analyses for storms when aircraft data are available, creating a synthesis of aircraft-, ground-, and satellite-based observations. TC analyses produced using HEDAS can provide input on how to improve the use of existing IFEX observations for model initialization, assess the value of new instrumentation, explore advanced data assimilation techniques, and provide a bridge between research and operational applications. For example, HEDAS demonstrated the importance of accounting for the dropsonde location as the instrument descends (Aberson et al. 2017)—a technique that has been transitioned into the operational HWRF.

Additional HEDAS developments have been designed to better represent the inner-core vortex structure and evolution. Some examples include: assimilating observations in a storm-relative framework (Aksoy 2013), increasing cycling frequency, varying

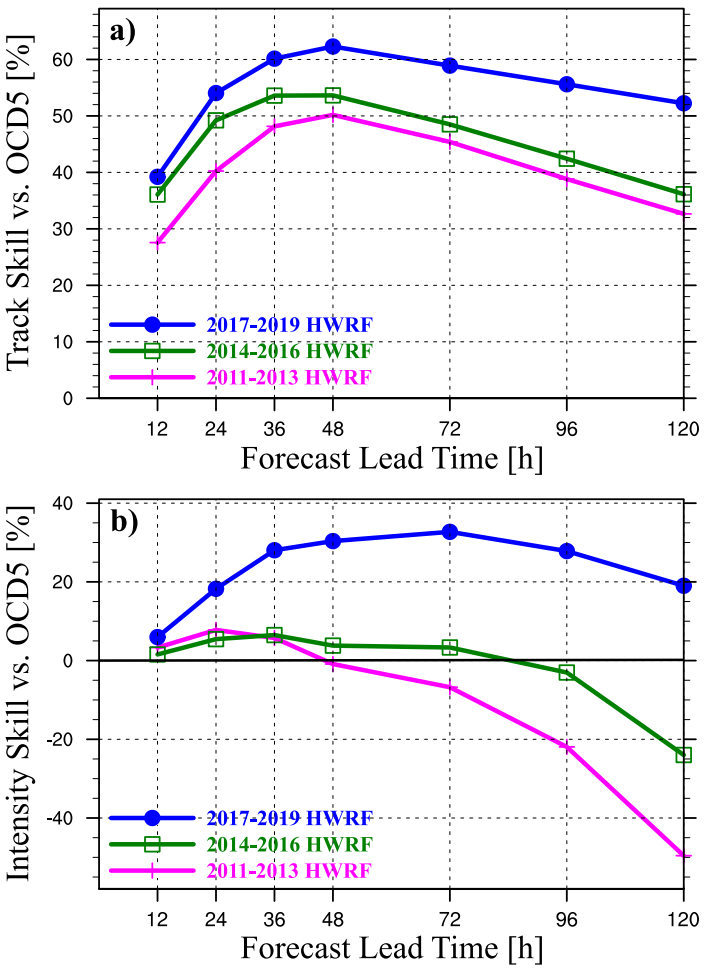

Fig. 3. Evolution of 12–120-h (a) track and (b) intensity skill for HWRF relative to NHC's climatology-persistence skill baseline (OCD5), composited for cases for three 3-yr periods: 2011–13, 2014–16, 2017–19.

localization radii (i.e., distance at which observations are allowed to influence the analysis), testing of new data assimilation methods (Steward et al. 2017, 2018), improving data quality control, and better identifying "outlier" observations.

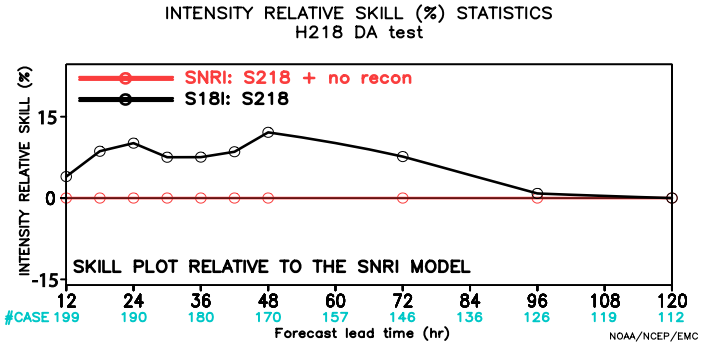

Fig. 4. The combined impact of all reconnaissance data on the intensity skill in a preimplementation version of the 2019 operational HWRF Model. The baseline (red) has no reconnaissance assimilation, while the operational version (black) has assimilation of TDR, dropsondes, flight-level, and SFMR data.

Designing new observing strategies. Advances in modeling and data assimilation create opportunities to reassess the use of existing aircraft platforms and distribution of expendables such as dropsondes (expendable instrument platforms deployed from the aircraft that measure pressure, temperature, humidity, and wind as they fall to the ocean). One method for reassessment is an observing system experiment (OSE), where assimilation of existing data can be tested and refined to optimize model analyses and provide insight into how to better integrate the information they provide into an operational model framework. For example, with the recent capability to transmit full-resolution (~1,000 vertical levels) dropsonde data that contain accurate position information compared to the legacy formatting (only ~20 mandatory and significant pressure levels), OSEs with dropsondes provided preliminary guidance for determining how many and which vertical levels should be assimilated to maximize the impact of these data on HWRF analyses and subsequent forecasts (Sellwood et al. 2020). Another OSE demonstrated that dropsondes deployed at altitudes higher than the P-3 (e.g., the Global Hawk) improved track and intensity forecasts for Hurricane Edouard (Christophersen et al. 2017).

Meanwhile, observing system simulation experiments (OSSEs) can demonstrate the potential impacts of hypothetical observations and help optimize sampling strategies. For example, the potential benefits of TDR data on assimilation were first demonstrated in an OSSE by Aksoy et al. (2012). In 2018, an OSSE also motivated a change in the sampling strategies of G-IV synoptic surveillance missions (Ryan et al. 2018). Traditionally, these missions focused on the large-scale environment around TCs for improved performance in track forecasts. The OSSE found that G-IV dropsondes had the largest positive impact on track forecasts when released in the transition region between the inner TC vortex and the near-storm environment (typically ~150 km from the center, though storm-size dependent). As a result of this study, NHC implemented an inner circumnavigation (typically ~150 km from the center) of dropsonde releases first during G-IV synoptic surveillance missions around Hurricane Florence (2018), and it has since become standard in surveillance flight tracks.

Model evaluation and development. Observations collected during IFEX provide the means for evaluating models beyond the traditional track and intensity metrics by detailed comparison of observed and modeled TC structures (Hazelton et al. 2018, 2020). For example, an evaluation using near-real-time TDR data has demonstrated the ability of a high-resolution model (e.g., HAFS in Fig. 5) to capture structural features [e.g., of the radius of maximum wind (RMW), eye, eyewall, and precipitation] of the inner core of Hurricane Laura (2020). The availability of TDR data in near–real time has already proven to be an invaluable tool for model evaluation, and future efforts will focus on transitioning real-time evaluation products that will allow forecasters the ability to compare models against observations while storms are ongoing.

Model evaluation using observations has also led to improved parameterization schemes, and subsequently forecasts, through the development of a framework to provide and test

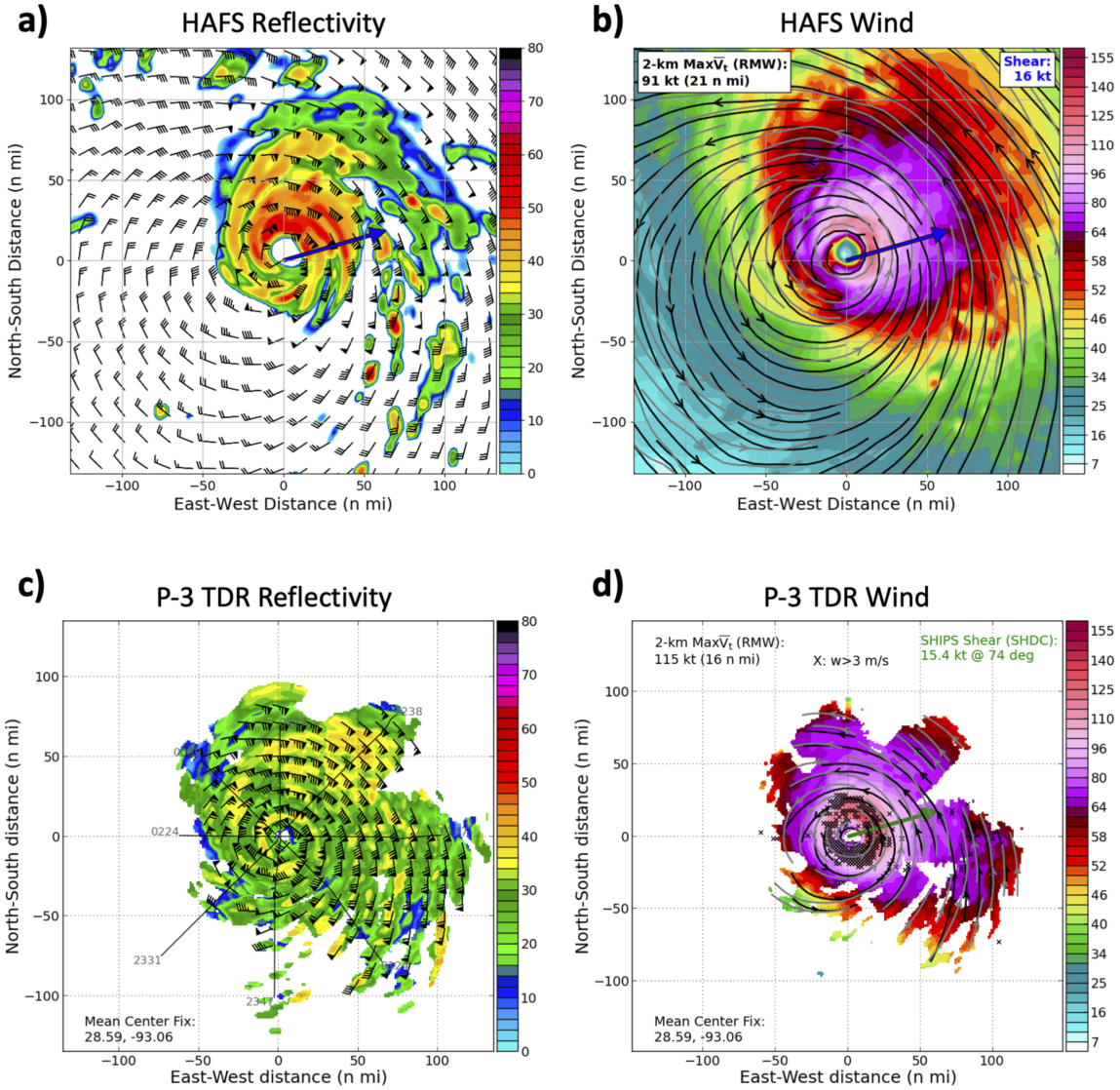

Fig. 5. (a) 2-km reflectivity (dBZ) and wind barbs (kt) from a 72-h forecast of the Hurricane Analysis and Forecast System (HAFS) of Hurricane Laura, initialized 0000 UTC 24 Aug 2020. The blue arrow shows the 850–200-hPa wind shear vector. (b) 2-km wind speed (kt), 2-km streamlines (black), and 5-km streamlines (gray) from the same 72-h forecast. The blue arrow shows the 850–200-hPa wind shear vector. (c) P-3 TDR observed 2-km reflectivity (dBZ) and wind barbs (kt), valid during the period from 2238 UTC 26 Aug to 0224 UTC 27 Aug 2020. (d) P-3 TDR observed 2-km wind speed (kt), 2-km streamlines (black), and 5-km streamlines (gray). The green arrow shows the 850–200-hPa wind shear vector from SHIPS.

observation-based estimates of physical parameters (Zhang et al. 2012). This framework was applied to HWRF's PBL parameterization scheme, in which the vertical eddy diffusivity was modified based on in situ observations of turbulent fluxes and vertical gradients of wind velocities in the TC PBL collected before (pre-2005) and during IFEX (Gopalakrishnan et al. 2013; Zhang et al. 2015). Likewise, observation-based improvements were also made to the parameterization of horizontal turbulent mixing in HWRF (Zhang and Montgomery 2012). These modifications improved vortex-scale, convective-scale, and boundary layer processes in PBL parameterizations that produced more realistic model TC structures consistent with observations (Zhang et al. 2015, 2017b; Bu et al. 2017; Zhang and Rogers 2019), while also reducing HWRF intensity biases (Zhang et al. 2015; Zhang and Marks 2015; Zhang et al. 2018a).

Finally, the diabatic heating associated with the formation, growth, and dissipation of hydrometeors is one of the primary driving forces of TC intensity changes, but most microphysics

schemes (which represent the collective effects of these processes) are not built for TCs. Data from cloud and precipitation probes on the P-3s obtained above the freezing level (5–7 km) were used to evaluate the ice particle size distribution (PSD) in microphysics schemes and showed that gamma functions more accurately reproduce observations than exponential functions (Leighton et al. 2020). Work is underway to understand how a more accurate parameterization of PSD in numerical models could lead to better intensity and rainfall forecasts.

IFEX goal 2: Develop and refine measurement strategies and technologies that provide improved real-time monitoring of TC intensity, structure, and environment

Near-real-time Doppler radar analyses. Automation of TDR data quality control, in conjunction with an established wind synthesis method (Gamache 1997; Reasor et al. 2009), has made possible the real-time transmission to NCEP of quality-controlled Doppler velocity data and the instantaneous archival of 3D analyses of TC wind and reflectivity structure. While the routine transmission of coarse-resolution analyses began in 2010, the benefits of these research-quality TDR analysis datasets have been realized in three important new ways within the past five years.

Increases in computational processing power and satellite communication bandwidth on the NOAA aircraft have led to real-time transmission of high-resolution (2-km horizontal spacing), 3D analysis datasets. This includes transmission of TDR data during G-IV surveillance missions since 2013. Through continued improvements in the automated quality-control process, the coverage of analyzed meteorological wind and reflectivity has increased, and nonmeteorological artifacts are mostly eliminated in most TC scenarios.

In addition to model evaluation (Fig. 5), another benefit of near-real-time TDR analysis is in providing enhanced situational awareness for scientists while missions are ongoing. After each flight segment through (or around) the TC center, publicly available graphics are automatically created highlighting structural aspects of the TC, like radius–height azimuthal-mean structure, flow and precipitation asymmetry, and vortex center tilt with height (examples of real-time TDR analyses for Hurricanes Laura and Teddy in 2020 are shown in Figs. 6 and 7). These real-time graphics can guide modifications to the aircraft sampling strategy that minimize spatial gaps in radar coverage of the circulation and help to achieve mission objectives.

Beginning with the 2018 Atlantic hurricane season, the TDR analysis data have also been available operationally for viewing within the AWIPS-II display system (example in Fig. 8) that is used by NWS to synthesize and view observational and model data. Within approximately an hour of a P-3 pass of a TC center, NHC now has access to the full 3D wind structure of the eyewall region and beyond. Although the analyses are currently limited to structure above 0.5-km altitude, and thus cannot provide direct estimates of surface wind, hurricane specialists have cited the TDR data in official NHC forecast discussions of Hurricane Humberto and Tropical Storm Jerry in 2019 in assessments of structure (e.g., vortex center tilt with height) and to provide context for flight-level and SFMR measurements that are available only along the flight track. To further meet NHC's needs, one research application in development is the use of TDR to estimate surface wind speed and to provide enhanced guidance on wind speed radii estimation by taking advantage of the combined coverage of P-3 and G-IV flight patterns.

Doppler wind lidar. As the utility of TDR analyses becomes widely recognized, it is important to fill the remaining data-sparse regions temporally and spatially in the TC wind field. These regions include the lowest levels of the PBL and precipitation-free areas that cannot be adequately sampled by the TDR, such as the upshear portion of highly sheared TCs and moats between the eyewall and outer rainbands or secondary eyewalls. A scanning coherent 1.6-μm airborne Doppler wind lidar (DWL) was flown on the P-3 for portions of the 2015–18 seasons into 8 TCs (Table 2). The DWL is capable of collecting wind

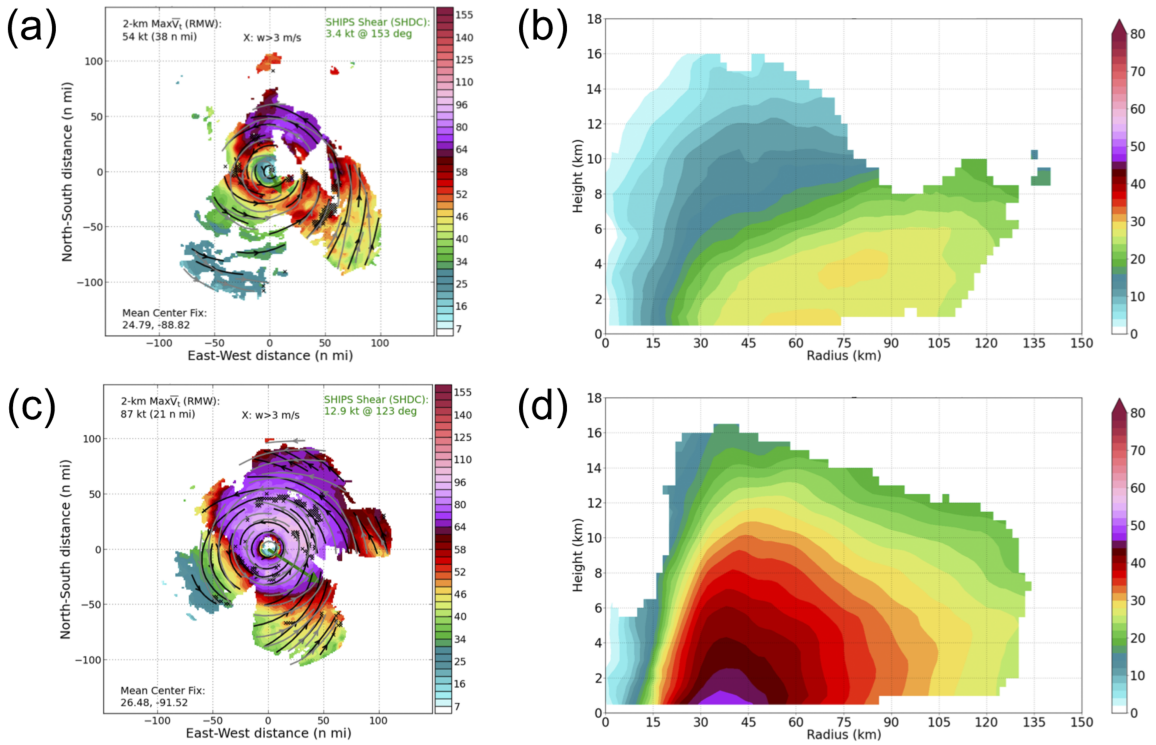

Fig. 6. Real-time TDR analyses of Hurricane Laura (2020) from P-3 missions during RI. (a) Flight-composite wind speed (kt) at 2 km (shaded), streamlines at 2 and 5 km (black and gray, respectively), and locations of updrafts > 3 m s^{-1} (hatched areas); and (b) azimuthal-mean tangential wind speed (kt) vs height for the period from 2230 UTC 25 Aug to 0155 UTC 26 Aug. (c),(d) As in (a) and (b), but 12 h later, from 1016 to 1449 UTC 26 Aug.

measurements above and below the aircraft when there is a sufficient concentration of aerosols and no optically thick clouds. A comparison of the P-3 DWL observations with other airborne wind observing systems validated the wind retrievals where observations overlapped (Bucci et al. 2018). For example, collocated dropsonde and DWL wind profiles showed a greater than 0.95 correlation for speed and 0.91 for direction. When combined with other observing systems, DWL augmented the observational coverage of the TC wind field (Bucci et al. 2018; Zhang et al. 2018b). Future work will focus on using DWL data to understand the dynamics and physical processes in the sparsely observed regions listed above, and assimilating it in models.

Dropsondes equipped with infrared sensors for measuring sea surface temperature. Surface fluxes of heat and moisture at the air–sea interface are tied to TC intensity as they are the main energy sources for the storm (e.g., Emanuel 1995; Shay et al. 2000; Ming and Zhang 2016). However, direct surface flux measurements in TCs are very difficult to obtain and, so far, have been limited to wind speeds below hurricane force. Alternatively, air–sea fluxes can be estimated using measurements of SST, 10-m wind speed, air temperature and humidity, and exchange coefficients through a bulk parameterization method. Either surface buoys or a combination of dropsondes with ocean expendables and/or other oceanographic instruments (e.g., underwater gliders) can provide these bulk flux estimates through collocated measurements of the above parameters. A standard dropsonde was modified to integrate an infrared (IR) sensor for SST measurements to collect collocated SST–atmospheric measurements. SST measured with this new type of dropsonde, referred to as an "IRsonde," showed good agreement with SSTs measured using ocean buoys in regions with weak rainfall (Zhang et al. 2017a).

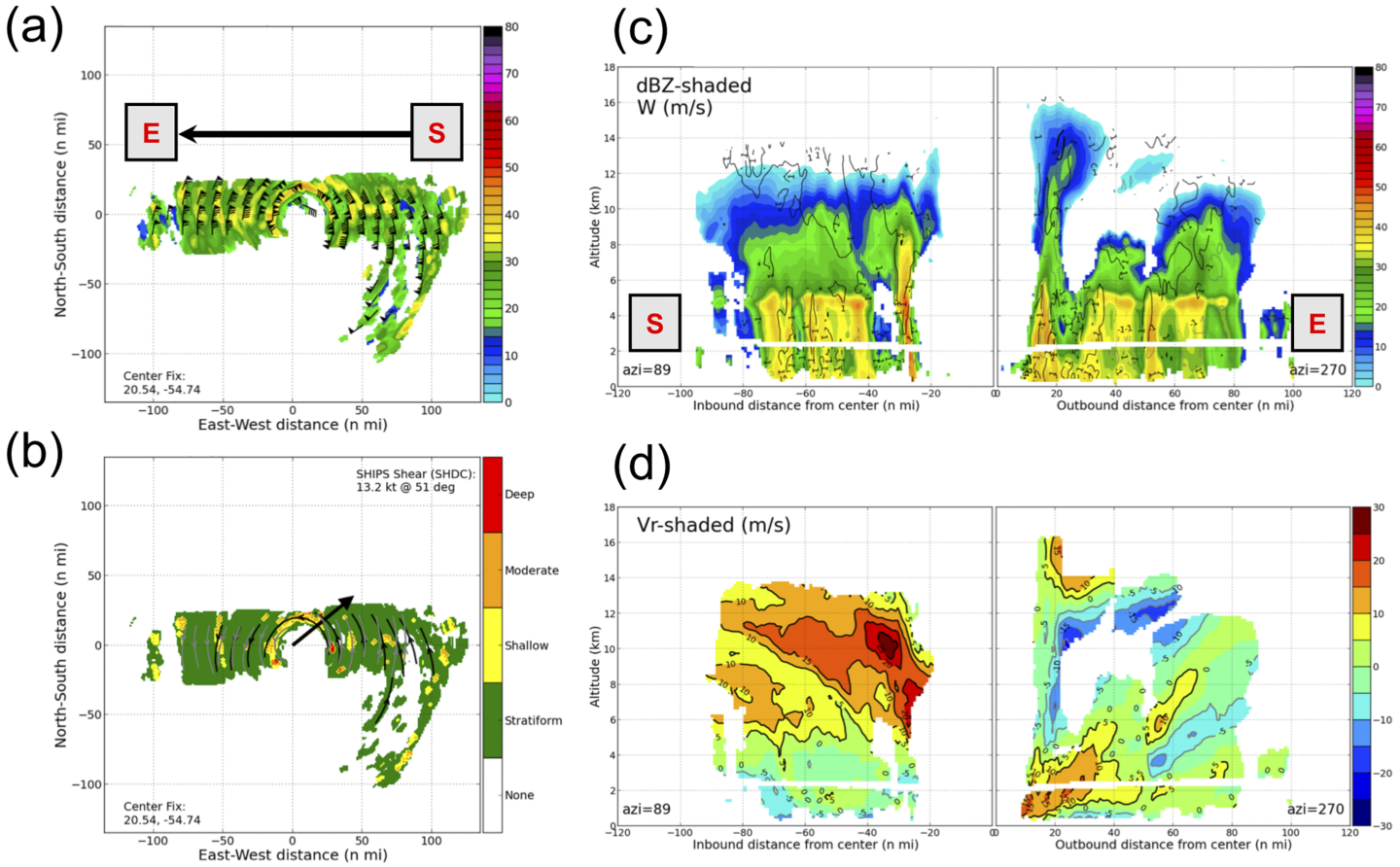

Fig. 7. Real-time TDR analyses from a pass of Hurricane Teddy from 0058 to 0211 UTC 18 Sep 2020 showing (a) 2-km reflectivity (dB*Z*) and wind (barbs, kt), (b) the precipitation type classification for convective ("deep," "moderate," "shallow") and stratiform, (c) the vertical profile cross section of reflectivity (shading, dB*Z*) and vertical velocity (contour, m s^{-1}; solid is upward motion, dashed is downward), and (d) the vertical profile cross section of storm-relative radial velocity (m s^{-1}). The red "S" indicates the start of the cross section, and the red "E" indicates the end, with the arrow in (a) showing the direction of the cross section and aircraft center pass.

sUAS. In 2014, the first use of air-deployed small uncrewed aircraft systems (sUAS) was in major Hurricane Edouard (Cione et al. 2016). Two successful deployments of the Coyote sUAS platform sampled the eye/eyewall and boundary layer inflow regions of the TC. These ground-breaking missions collected data in a critically important, yet sparsely sampled area of the TC where crewed aircraft are unable to fly. More recently, analyses of observations from seven Coyote flights into Hurricanes Maria (2017) and Michael (2018) were also conducted (Cione et al. 2020). A total of nine sUAS missions were flown in three major hurricanes. In all cases, high-resolution PBL measurements of pressure, temperature, relative humidity, wind, and estimates of SST were recorded and will be valuable for shedding important insights into air–sea exchange processes, PBL turbulent structures, and optimizing physical parameterizations in coupled ocean–atmosphere TC modeling systems.

SFMR. The SFMRs on the P-3 and 53rd WRS aircraft obtain surface wind speed estimates at nadir below the aircraft when flying straight and level. The SFMR relies on comparisons to dropsondes to determine the relationship between the raw observations and wind speed (Klotz and Uhlhorn 2014). When dropsondes are released in the eyewall, they are carried by the storm circulation away from where the SFMR collects observations, making direct comparisons between the SFMR and dropsondes difficult. Therefore, a flight pattern was designed to overfly the splash location of dropsondes released in the eyewall to obtain direct

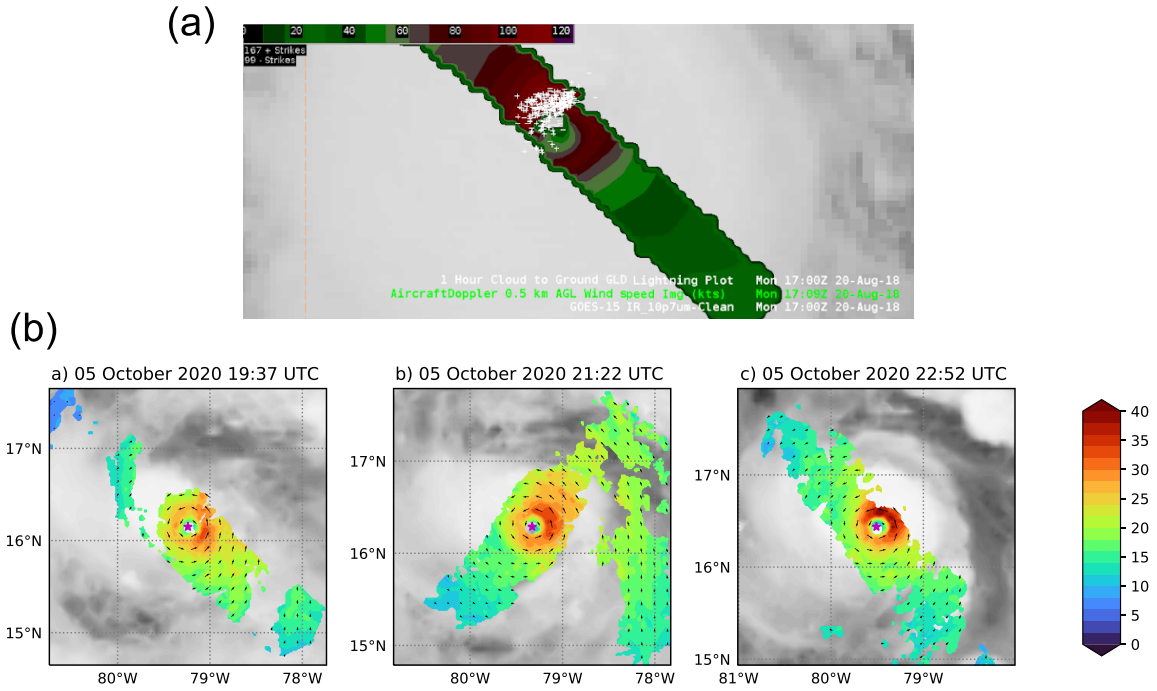

Fig. 8. (a) Example from AWIPS-II display of TDR data from Hurricane Lane in the central Pacific at 1700 UTC 20 Aug 2018, overlaid with TDR 0.5-km wind speed (kt, shading), *GOES-15* infrared satellite imagery, and 1-h cloud-to-ground lightning from the Global Lightning Detection Network (GLD360) (figure courtesy of Stephanie Stevenson, NHC). This was one of the first opportunities for hurricane specialists at NHC and the Central Pacific Hurricane Center to view TDR data in AWIPS-II while the P-3 was still in flight. (b) Sequence of 2-km Earth-relative wind analyses (m s^{-1}) from the TDR showing the RI of Hurricane Delta (2020) for three passes over ~3 h, produced from the files formatted for AWIPS-II.

spatial collocations of SFMR and dropsondes. These observations will be used to improve the operational SFMR algorithm at high wind speeds in the eyewall of major hurricanes.

When flying through a TC it is also common for the aircraft to exceed the SFMR's thresholds on the aircraft pitch and roll angles, at which point the SFMR does not report useable data. This occurs as the aircraft descends (ascends) on a pressure surface into (out of) the eyewall of strong hurricanes, a critical location to obtain surface wind speed estimates. Data have been collected to develop a correction to the SFMR that accounts for pitch and roll angle variations (Holbach et al. 2018). This experiment collected data at constant aircraft roll angles in regions of constant surface conditions over a broad range of surface wind speeds. A second SFMR was also mounted on the P-3 aircraft oriented perpendicular to the operational unit to study the impacts of pitch angle on the SFMR measurements.

IFEX goal 3: Improve the understanding of physical processes important in intensity change for a TC at all stages of its life cycle

With several decades worth of TC missions flown by NOAA aircraft, there is a tremendous database of TDR, dropsonde, flight-level, SFMR, and ocean buoy observations that has been accumulated. Such a database allows for analyses of individual cases to provide in-depth exploration of physical processes and their evolution in time, and composite studies to identify statistically robust differences in vortex- and convective-scale structures of TCs encountering a variety of environmental conditions and structure and intensity changes. Examples of the research since R13 are summarized below.

Characterizing TC inner-core structure and intensity change. A composite analysis of TDR data for intensifying versus nonintensifying TCs found that intensifying TCs were

associated with a ringlike vorticity structure inside the RMW, lower vorticity in the outer core, and a stronger and deeper radial inflow layer (into the center) compared to steady-state TCs (Rogers et al. 2013b). Similar relationships were found for composites of flight-level data, along with higher inner- and outer-core moisture for intensifying TCs (Martinez et al. 2017). When composited for TCs experiencing vertical wind shear, TDR data also confirmed principal features of the wind shear-induced TC asymmetry documented in prior numerical and observational studies; e.g., circulation center tilted downshear in the vertical, downshear-right (DSR) convective initiation, and a subsequent downshear-left (DSL) precipitation maximum (Reasor et al. 2013). Case-study analyses were conducted for the record-breaking rapidly intensifying east Pacific Hurricane Patricia (Rogers et al. 2017), including a novel analysis of TDR and dropsonde data (Martinez et al. 2019) that found that Patricia's RI was related to the distribution of diabatic heating and mixing across the eye–eyewall interface.

TC intensity change in vertical wind shear. The effect of moderate values of vertical wind shear (~5–10 m s^{-1} between 850 and 200 hPa) on TC structure and intensity is a source of considerable forecast uncertainty (Bhatia and Nolan 2013; Zhang and Tao 2013) and has been recognized by NHC as a high priority for research (Sumwalt et al. 2017). Recent IFEX research addressed this priority, focusing on characterizing the multiscale structures associated with intensity change in shear, with the goal of better understanding the physical processes underlying intensity change in these environments.

The emphasis of this work has been on 1) characterizing the structure and distribution of precipitation (and by extension latent heating) in a shear-relative and RMW-relative framework that are associated with TC intensification in shear and 2) identifying the multiscale structures that modulate precipitation. For example, analyses of P-3 data from individual cases (example from Edouard in Figs. 9a,b from Rogers et al. 2016; Susca-Lopata et al. 2015) and composites (Rogers et al. 2013b, 2015; Wadler et al. 2018a) have shown that, for intensifying TCs, the preferred radial location of the strongest convective cores, i.e., convective bursts, is inside the low-level RMW, with a more symmetric coverage of precipitation around the TC center (Alvey et al. 2015; Rogers et al. 2016).

Associated with the increase in precipitation symmetry is the preference for intensifying TCs to have deep convection in the upshear-left (USL) quadrant [Figs. 9a,b; Rogers et al. 2016; also observed by Wadler et al. (2020) in Hurricane Michael]. Composited TDR data showed that convective bursts in the USL quadrant of intensifying TCs had updrafts that peaked with a higher magnitude, at a higher altitude, and with higher echo tops, than nonintensifying TCs (Wadler et al. 2018a). The importance of deep convection extending into the USL quadrant was also confirmed in numerical modeling studies (Chen and Gopalakrishnan 2015; Leighton et al. 2018; Rios-Berrios et al. 2018), and in an investigation of vertical mixing in the PBL (Zhang and Rogers 2019).

Shear-relative distributions of midlevel relative humidity, low-level equivalent potential temperature (θ_e), SST, and vortex tilt modulate the azimuthal distribution of precipitation and latent heating around the TC center. Dropsonde data (Zawislak et al. 2016; Nguyen et al. 2017) and subsequent modeling studies (e.g., Alvey et al. 2020) showed that a more-humid midlevel upshear environment was an important factor in sustaining precipitation coverage upshear, increasing precipitation symmetry and favoring intensification (Fig. 10). For example, in Edouard an increase in the mid- to upper-level humidity was observed in the USL quadrant as the storm intensified between 12 and 15 September (Fig. 9d).

The approach of examining factors responsible for modulating precipitation structure and distribution in a sheared environment was also applied to weaker TCs, including tropical depressions, where circulation centers are often misaligned and dry air plays in

important role in suppressing convection. Rogers et al. (2020) combined P-3 TDR and deep-layer GH dropsonde data to identify a multiscale cooperative interaction between deep (20-dBZ echo tops > 10 km) and moderate (echo tops between 6 and 10 km) convection on the downshear side of a TD that became Hurricane Hermine (2016). The local environment had become moistened and stabilized through successive cycles of convective and stratiform precipitation. The interaction between deep and moderate convection lowered the altitude and increased the magnitude of the peak vertical mass flux (Fig. 11), fostering a persistently aligned vortex that marked the onset of intensification to hurricane strength.

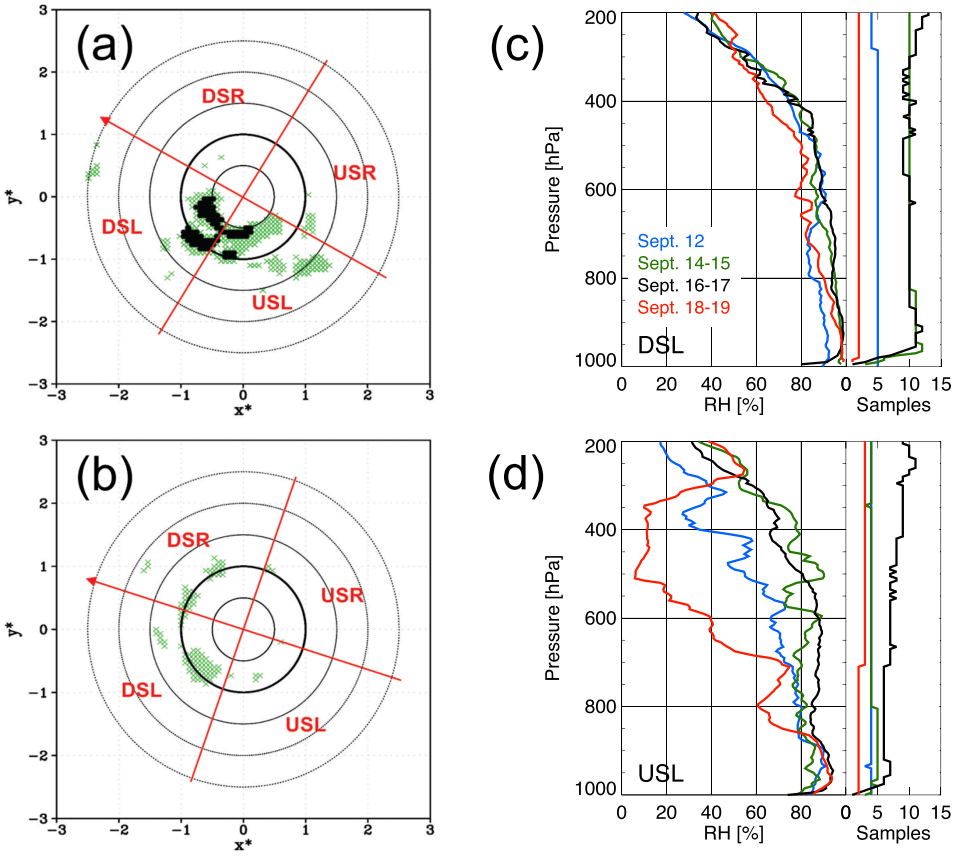

Fig. 9. For Hurricane Edouard (Fig. 1), accompanying locations of peak updrafts of greater than 3 (green) and 5 m s^{-1} (black), i.e., "convective bursts," between the 8- and 16-km layer from the TDR for passes during the (a) 14 (intensifying) and (b) 16 (steady state) Sep missions relative to the 850–200-hPa vertical wind shear [downshear right (DSR), downshear left (DSL), upshear left (USL), and upshear right (USR)] and in an Earth-relative coordinate system normalized by the low-level (2-km) RMW (x^*, y^*) (adapted from Rogers et al. 2016). (c),(d) The mean relative humidity profiles and number of contributing samples within 200 km of the center of Edouard for the DSL and USL quadrants, respectively, from the four GH missions (adapted from Zawislak et al. 2016).

Boundary layer processes and air–sea interaction. In addition to modulating the azimuthal distribution of precipitation (diabatic heating), vertical shear can also govern the low-level θ_e (temperature and moisture) distribution through recovery processes of the PBL. Composite dropsonde analyses of PBL structure were used to show an energy cycling process (Molinari et al. 2013; Zhang et al. 2013) where convection is triggered DSR in the presence of a maximum in θ_e, convective downdrafts bring down cool and dry air to the PBL and lower θ_e in the DSL and USL quadrants, and air parcels reacquire high θ_e from air–sea fluxes as they rotate through the USL and upshear-right (USR) quadrants. Stronger surface fluxes upshear were a key feature distinguishing intensifying from nonintensifying TCs in a composite analysis (Nguyen et al. 2019) and case studies (Jaimes et al. 2015; Zhang et al. 2017a; Wadler et al. 2018b; Zhang and Rogers 2019).

Composites of buoy data also showed larger surface fluxes in intensifying storms than in weakening ones due to air–sea humidity differences (Cione et al. 2013). Higher SST favors the increase of surface fluxes, which in turn recover downdraft-induced low-θ_e air in TCs undergoing RI (Zhang et al. 2017a; Wadler et al. 2020). These impacts of boundary layer recovery on surface fluxes and RI onset are important in statistical–dynamical prediction schemes and numerical models (Kaplan et al. 2015; Zhang et al. 2017a).

Kinematic structural differences of the PBL between RI and non-RI TCs have also been identified in IFEX dropsonde data and confirmed by numerical models. Intensifying TCs have a deeper and stronger supergradient PBL jet (i.e., the part of the horizontal wind that exceeds gradient wind balance), higher inertial stability (i.e., the resistance of the storm vortex structure to change from other forces), and stronger turbulent mixing in the eyewall region than nonintensifying cases (Montgomery et al. 2014; Rogers et al. 2016; Zhang et al. 2017b; Ahern et al. 2019). Composites of HWRF forecasts have shown that intensifying TCs have stronger PBL inflow in the eyewall region, with stronger PBL convergence closer to the center, than nonintensifying TCs (Zhang et al. 2017b)—consistent with the notion that forced convection and strong updrafts are preferentially observed inside the RMW in intensifying TCs (Rogers et al. 2013b). In a sheared storm, the azimuthal distribution of PBL inflow and convergence also affects the extent of asymmetry of shallow and moderately deep convection, with inflow being more symmetric for TCs undergoing RI (Zhang and Rogers 2019). The stronger inflow also acts to advect more angular momentum toward the center and spin up the primary circulation in the PBL, favoring RI (Smith et al. 2017; Zhang and Rogers 2019).

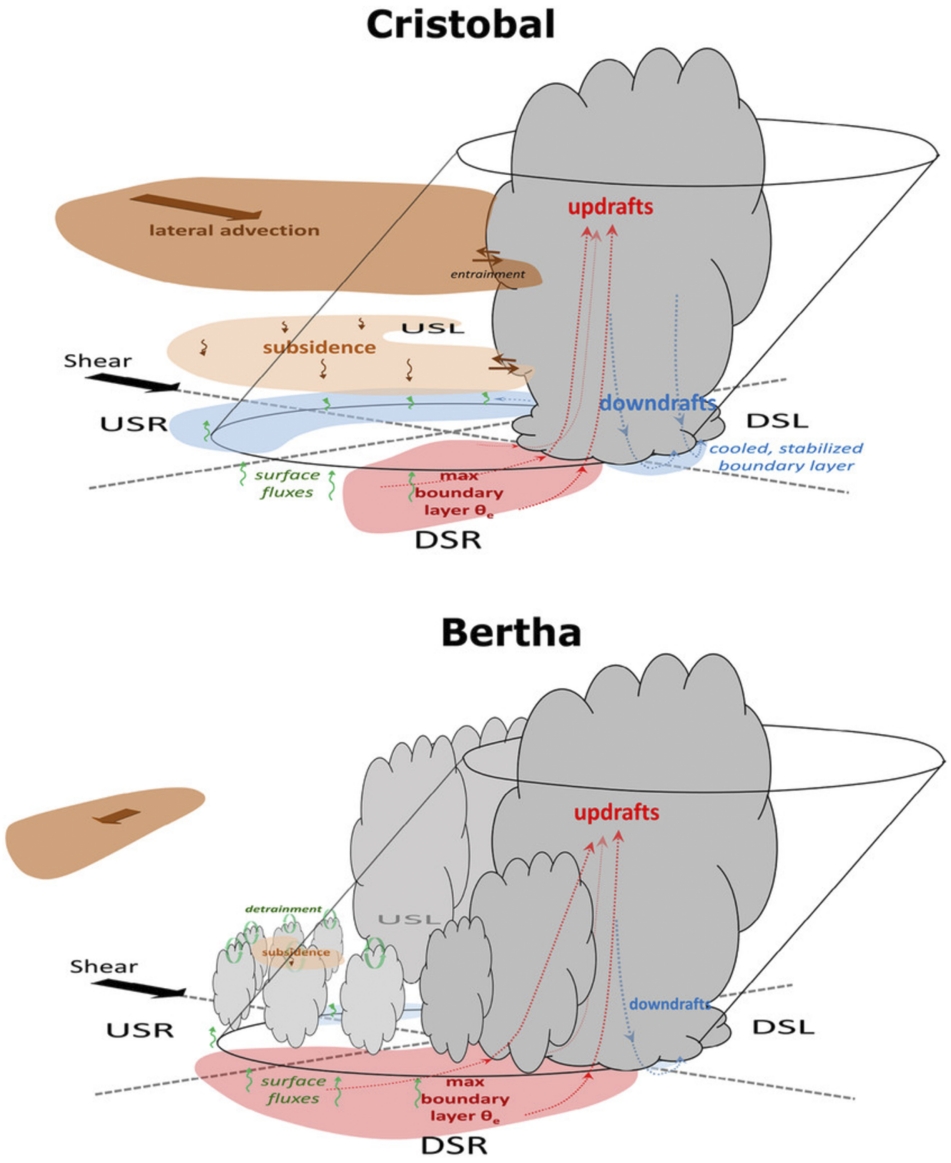

Fig. 10. Three-dimensional schematics summarizing the hypothesized hindrances to precipitation symmetry in TCs. (top) A case with more-asymmetric precipitation (Cristobal 2014), which is less favorable for intensification. (bottom) A case with more-symmetric precipitation (Bertha 2014), which is favorable for intensification. Lateral advection of environmental dry air on the upshear side (USL, USR) of TCs, subsidence upshear, and weak surface fluxes upshear that inhibit PBL recovery all contribute to hinder symmetrization of precipitation in a sheared TC. Adapted from Nguyen et al. (2017).

The transition of the TC boundary layer structure that occurs at and immediately after landfall was investigated in Hurricane Irene (Alford et al. 2020). Irene's boundary layer structure evolved differently in the eyewall and rainband regions, which may have implications for where the strongest overland wind occurs in a landfalling TC.

Secondary eyewall formation and eyewall replacement cycles. Another period of the TC life cycle is the mature stage when secondary eyewall formation (SEF), typically followed by an

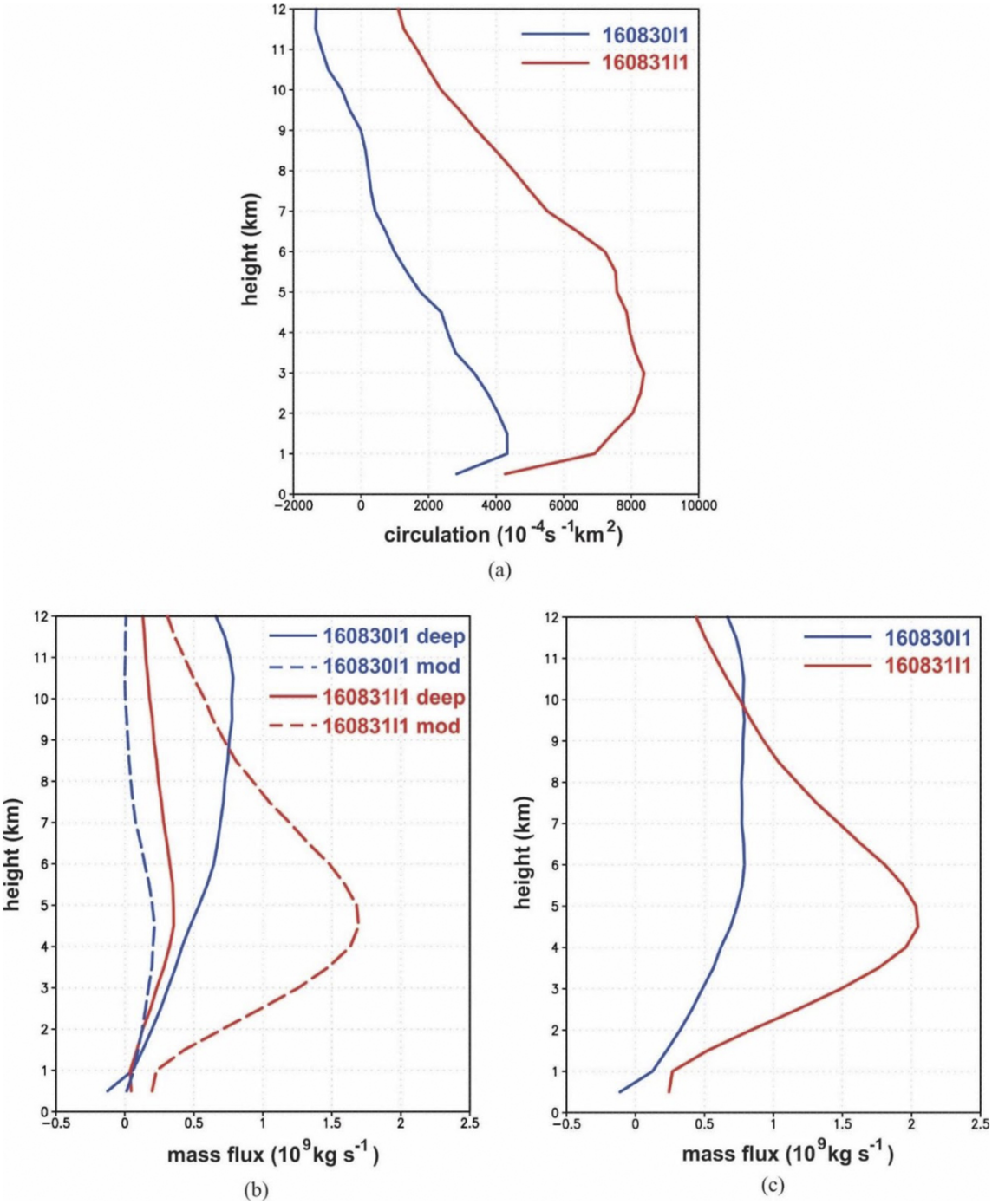

Fig. 11. (a) Vertical profile of total circulation (×10^{-4} s^{-1} km^{-2}) per center pass from two missions by the P-3 in a 1.25° × 1.25° box incorporating low-level circulation center and downshear environment in Hermine. Values averaged from three center passes during missions centered at ~2000 UTC 30 Aug 2016 in Tropical Depression 9 (mission 160830I1; blue line) and ~2000 UTC 31 Aug 2016 in Tropical Storm Hermine (mission 160831I1; red line). (b) Contributions to aggregate vertical mass flux (×10^9 kg s^{-1}) per center pass from regions classified as deep (solid) and moderate convection (dashed) for mission 160830I1 (blue) and mission 160831I1 (red). (c) As in (b), but for the sum of mass flux from deep and moderate convection for each mission. Note pronounced lowering in altitude and increase in magnitude of peak mass flux between two missions, with primary contribution from moderate convection during the later mission. Adapted from Rogers et al. (2020).

eyewall replacement cycle (ERC), can occur. TDR observations were used to hypothesize that SEF can result from PBL convergence driven by a mesoscale descending inflow jet originating from a stratiform precipitation region (Didlake et al. 2018), while dropsonde observations have

shown that SEF can occur in a region characterized by a local maximum in the PBL inflow associated with agradient forcing (i.e., a force imbalance between the inward-directed pressure gradient force and outward-directed centrifugal and Coriolis forces) (Abarca et al. 2016). Other studies have hypothesized that changes to the azimuthal-mean flow brought on by the interaction between wavelike perturbations of vorticity, referred to as vortex Rossby waves, with the mean flow can lead to SEF (Dougherty et al. 2018; Guimond et al. 2020). TDR observations of two consecutive periods of SEF in Hurricane Irma (2017) showed that multiple processes produce SEFs (Fischer et al. 2020). The first SEF event (Fig. 12) was driven by both a mesoscale descending inflow jet and vortex Rossby waves interacting with the mean vortex structure, while the second SEF occurred in a region of enhanced convergence that arose from processes consistent with a force imbalance in the PBL as well as continued vortex Rossby wave activity.

While TCs typically weaken during ERCs, recent work has found that in some cases the TC will fail to weaken as the ERC completes (Dougherty et al. 2018), or even rapidly intensify

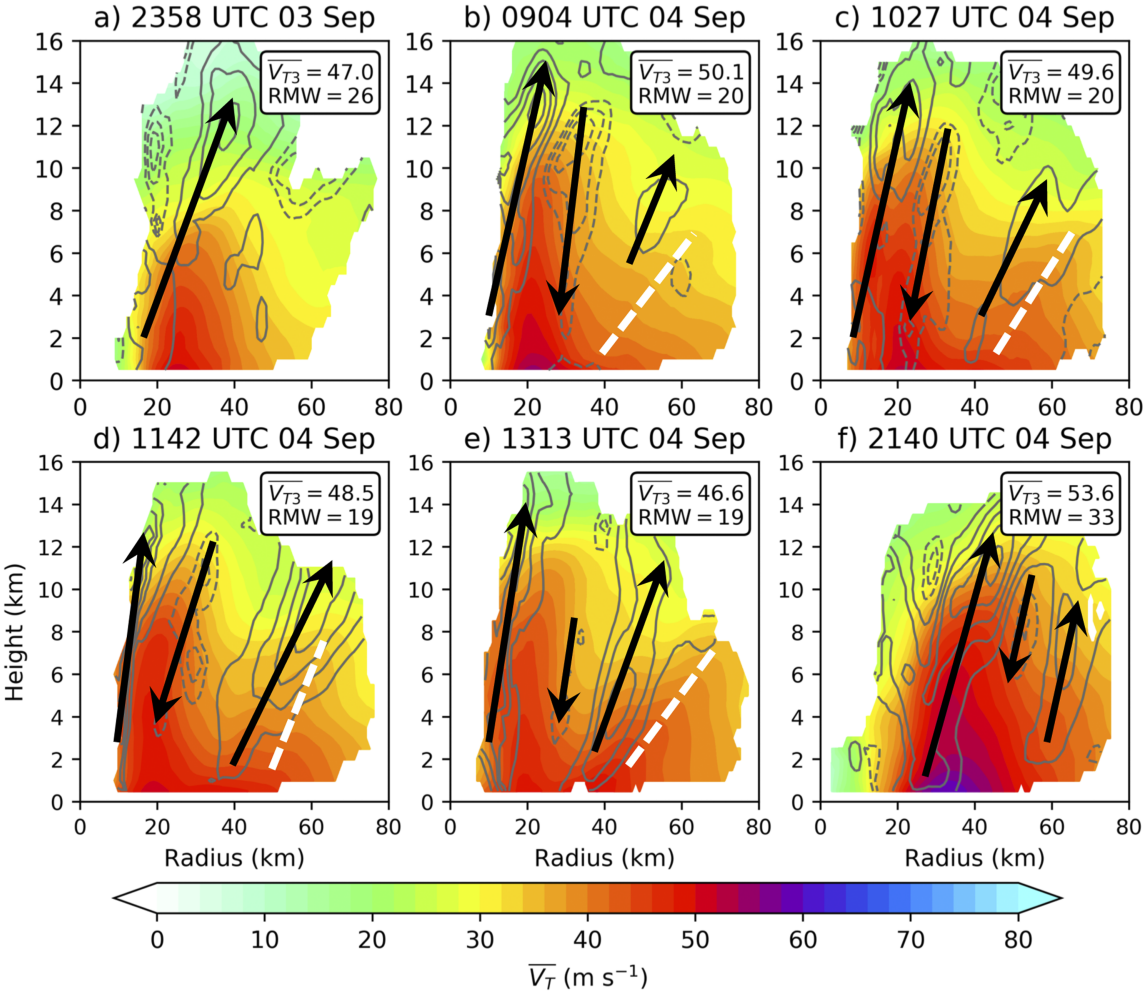

Fig. 12. Radius–height depiction of SEF/ERC in Hurricane Irma (2017). Azimuthally averaged tangential (V_T; m s^{-1}; shaded) and vertical wind speed (contours) obtained from six center passes by the P-3 on 3–4 Sep. Positive vertical velocity values are shown in the solid contours every 0.5 m s^{-1}, while negative vertical velocity values are shown in the dashed contours every 0.2 m s^{-1}; solid arrows indicate the direction (upward/downward) of the vertical motion. The inset of each panel depicts the magnitude of the maximum azimuthally averaged tangential wind speed at a height of 3 km (V_{T3}; m s^{-1}) and the radius of V_{T3} (RMW; km). For each flight, only radii with at least 33% azimuthal coverage are shown. (c)–(e) Note the development and contraction of outer maximum in tangential wind and vertical wind speed (the secondary eyewall, denoted by the white dashed lines), beginning at ~50–55-km radius and contracting to ~40-km radius over ~3-h period. Adapted from Fischer et al. (2020).

(Fischer et al. 2020). The variability of the temporal scales of ERCs has also been noted, as the duration of an ERC can range from less than 12 h to multiple days (Molinari et al. 2019; Fischer et al. 2020). Furthermore, the nature of TC convective asymmetries during ERCs has been assessed (Didlake et al. 2017; Dougherty et al. 2018; Didlake et al. 2018; Fischer et al. 2020). For example, Didlake et al. (2017) discovered that updrafts in the outer eyewall tend to occur downwind of updrafts in the inner eyewall.

Looking to the future

During the past 16 years, IFEX has contributed to substantial advancements in our ability to observe, understand, and predict TC structure and intensity. More effective assimilation of airborne data into numerical models, along with the use of these data to improve the representation of physical processes in these models, have led to demonstrable improvements in intensity forecast guidance. New observing technologies and the improved ability to quality control, analyze, and visualize aircraft observations have significantly enhanced the ability to assess TC structure and intensity in real time. Finally, case-study and composite-based research studies have led to new insights into TC structure and intensity change processes (see "Measures of success" sidebar), laying the groundwork for forecast improvements now and in the future.

These advancements in our understanding and prediction of TCs have been made possible through partnerships between the operational requirements and research opportunities within and outside NOAA that have formed the foundation of IFEX. As these partnerships continue to strengthen, there is an even greater emphasis on using airborne observations to address the broad array of forecast challenges facing the operational community. For example, many of the significant landfalling TCs of the past several years (Table 1) formed and intensified, some rapidly, within a day or two of landfall. These "short-fuse" storms offer emergency managers and the public little time for preparation. As highlighted in Table 1, they bring dangerous hazards—notably, storm-surge inundation and extreme rainfall that are responsible for the majority loss of life in storms—beyond just high winds and tornadoes. While there has been much progress during the IFEX period, forecast guidance continues to be challenged to predict these hazards better, and the path to solving these challenges continue to be through improved skill in resolving TC characteristics themselves.

The partnership between IFEX and HFIP will continue to strengthen as each progresses into its next generation. During the next five years, HFIP will continue to seek progress toward improved TC prediction, but with a specific focus on more skillful forecasts of TC track, intensity, and structure out to 7 days (previously 5 days), more accurate genesis and RI forecasts, and improved probabilistic forecast guidance for all hazards, including better communication to the public of those risks.

Guided by these goals, IFEX will also evolve into its own next generation as it continues its support of HFIP and operations at NHC and EMC. This evolution will include a continued prioritization on flying TCs earlier in their life cycles, such as the preformation and depression stages where the observational record is lacking compared to the mature stage (Table 3, Fig. 2), and in TCs in marginal environments for intensification, where intensity change is less predictable (Bhatia and Nolan 2013). Observations from these flights will continue to fill gaps in our understanding of the interactions between a TC's environment and inner core, and the physical processes that drive genesis and intensification.

Likewise, at its core, IFEX will maintain the approach that has worked so well: the use of aircraft observations to improve the understanding of physical processes and their use in advancing data assimilation, numerical modeling, and OSE/OSSE systems that contribute to better TC forecasting. For example, observations will play a collaborative role in the development of HAFS—NOAA's next generation hurricane model and data assimilation package that will offer an operational analysis and 7-day guidance for TC genesis, track, intensity (including RI),

storm size, rainfall, and tornadoes. Observations will be critical in the production of a HAFS operational analysis as all available airborne and satellite data will be assimilated using new data assimilation advancements developed for HAFS. In turn, HAFS can be a tool for advancing knowledge of TC processes and theory through a combination of observations and model analyses. As for OSE/OSSEs, they will further evolve and determine the potential impact of new instrumentation and targeted observing strategies in model forecasts and resource utilization.

New observing strategies and instruments will continue to play a key role in sampling relatively undersampled storm processes and structures (e.g., PBL, microphysics, and turbulence, Fig. SB1). For example, remote sensors can be adopted on the P-3s and G-IV (or the Gulfstream G550 that NOAA is acquiring) to provide a more complete 3D picture of the TC structure, and to understand what modulates storm size; e.g., extent of the 34-, 50-, and 64-kt surface wind speed radii that get integrated into storm-surge models like the statistical Probabilistic Hurricane Storm Surge (P-Surge) model (Taylor and Glahn 2008). sUAS platforms released from the P-3s will fly longer (up to 4 h), providing invaluable situational awareness and real-time monitoring, and carry instruments that better characterize and model the typically undersampled processes in the PBL. The Wide-Swath Radar Altimeter (WSRA; PopStefanija et al. 2021), an already proven technology on the P-3, will transmit real-time observations of the ocean surface wave field, which help to understand the impacts of waves on PBL processes and coastal impacts, and improve situational awareness for marine forecasters during TCs. Data from cloud microphysics probes can be used to improve physics parameterizations, which drive model representation of precipitation structure and, subsequently, rainfall forecasts. And coordination with ground-based landfall observing teams and their array of instrumentation, such as mobile radars, profilers, towers, and ground weather stations, can aid with studying many aspects of landfalling TCs, such as the documentation of convective bands as they move inland (potentially causing tornadoes), as well as changes in the wind field as the TC comes ashore.

Observing strategies will also focus on validation of satellite measurements. Since 2018, IFEX has collaborated with the NOAA Joint Polar Satellite System (JPSS) program to release dropsondes from the G-IV for validating satellite retrievals of temperature and moisture soundings from the NOAA Unique Combined Atmospheric Processing System (NUCAPS). The need to understand, and improve upon, limitations in satellite observations of TCs will continue in the future as satellites will remain the primary means of observing TCs globally.

New and more frequent in situ ocean-profiling instruments are also necessary to understand the role of the upper-ocean thermal structure and air–sea interaction processes, especially when they coincide with atmospheric measurements (Fig. 13), and can be assimilated into atmosphere–ocean coupled models. For example, underwater ocean gliders are being deployed in the North Atlantic and Caribbean in a multi-institutional effort that includes AOML's Physical Oceanography Division. The gliders are underwater autonomous vehicles that provide targeted, real-time ocean profiling observations of temperature and salinity in the path of TCs (Domingues et al. 2019). Their operating locations make them easy targets for coordinating aircraft overflights, as was accomplished for the first time in Dorian (Fig. 13). Gliders not only provide valuable data for process studies, but they have also proven to improve operational TC forecasts (Dong et al. 2017), especially when their assimilation into coupled models are complemented by other standard ocean observations from buoys, ships, drifters, and floats.

APHEX: NOAA's next airborne hurricane field program.

With the above considerations in mind, the focus on "intensity forecasting" at the inception of IFEX is now a narrow scope within a broad expanse of forecast challenges and knowledge gaps that must be addressed at all stages of the TC life cycle, though especially in the genesis and early stages. With the IFEX priorities broadened beyond intensity to include structure

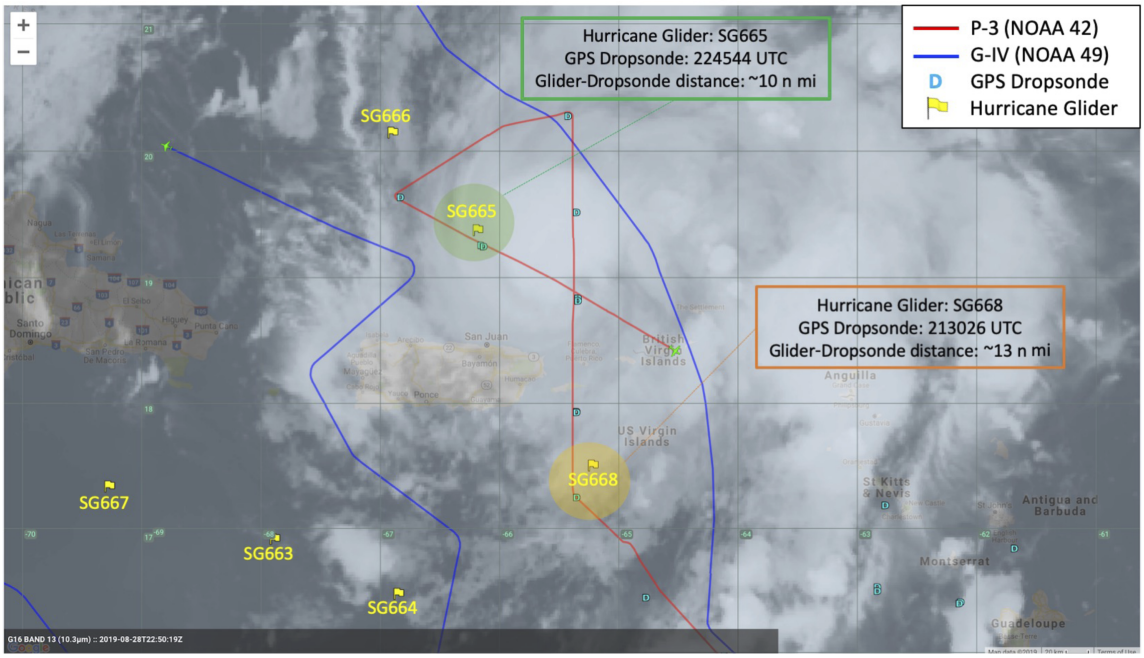

Fig. 13. P-3 (red) and G-IV (blue) flight tracks, P-3 dropsonde release locations (teal "D"), and hurricane glider locations (labeled in yellow with flags) overlaid with IR satellite imagery from Hurricane Dorian on 28 Aug 2019. Shaded circles indicate the coordinated glider–dropsonde measurements. Image is developed using a screenshot from NASA's Mission Tools Suite (MTS), which is used for real-time mission situational awareness during the field program.

and hazards, and with the focus of improving model analyses with observations (prioritized by HFIP through HAFS), the following modifications (highlighted in italics) to the IFEX goals will be made:

1) Collect observations that span the TC life cycle in a variety of environments for model initialization and evaluation.
2) Develop and refine measurement strategies and technologies that provide improved real-time *analysis* of TC intensity, structure, environment, *and hazard assessment*.
3) Improve the understanding of physical processes that *affect TC formation, intensity change, structure, and associated hazards*.

To reflect this broader emphasis, the IFEX acronym will be retired in favor of a new acronym: Advancing the Prediction of Hurricanes Experiment (APHEX).

Acknowledgments. Data collection for the hurricane field program would not have been possible without the incredible and heroic efforts of all the pilots, flight directors, navigators, engineers, technicians, mechanics, program managers, and leadership at NOAA/OMAO and their Aircraft Operations Center (AOC). We especially want to acknowledge the late Jim McFadden, former Chief of Programs at AOC, whose decades of leadership and dedication paved the way for the success and accomplishments of this program. IFEX also appreciates the courageous and tireless efforts of 53rd Air Force Reserve Weather Reconnaissance Squadron and the data they provide each season, as well as the staff at the unit of the Chief, Aerial Reconnaissance Coordination, All Hurricanes (CARCAH). Michael Brennan, James Franklin, and Ed Rappaport at NHC and Avichal Mehra and Vijay Tallapragada at EMC have also been instrumental and supportive partners who guide the priorities of this program and have

Measures of success

The success of IFEX has primarily been measured using three metrics. The first is the impact IFEX has had within the operational community through research-to-operational transitions. Many of these impacts were highlighted in IFEX goals 1 and 2, and reflect key contributions to the notable improvement in intensity forecasts over the past decade (Cangialosi et al. 2020).

The second measure gauges the breadth and impact of publications that have used NOAA aircraft data. Figure SB1a shows the number of published manuscripts since 2006 that included AOML/HRD authors and that used NOAA aircraft data (collected through IFEX research missions and operational flights), linked to each IFEX goal. Goal 3 ("physical processes") represents the largest number of manuscripts, followed by goal 1 ("model evaluation/initialization"), and then goal 2 ("real-time monitoring"). Goal 3 publications are further separated by various aspects of TC processes, both within their inner core and environment (Fig. SB1b). The most frequently published topics include those related to TC structure, intensity change, ocean and air–sea interaction, PBL, and precipitation. Fewer studies have been published on TC–environment interactions, turbulence, and microphysics—suggesting a need for additional focus on these topics in the future.

Though not entirely quantified in Fig. SB1 (as that figure only includes papers with HRD authors), the third metric is the extent to which IFEX data are used by researchers and forecasters outside of AOML/HRD. The airborne hurricane field program is a service to the entire research and operational community with a common goal of improving forecasts for the public. AOML/HRD maintains a decades-long archive of raw and quality-controlled, research-quality NOAA aircraft TC data on its web page (www.aoml.noaa.gov/hurricane-research-division/) and is continually trying to make data more useful to its users. Users are encouraged to contact AOML/HRD scientists to help facilitate their data needs and to collaborate on an experiment design.

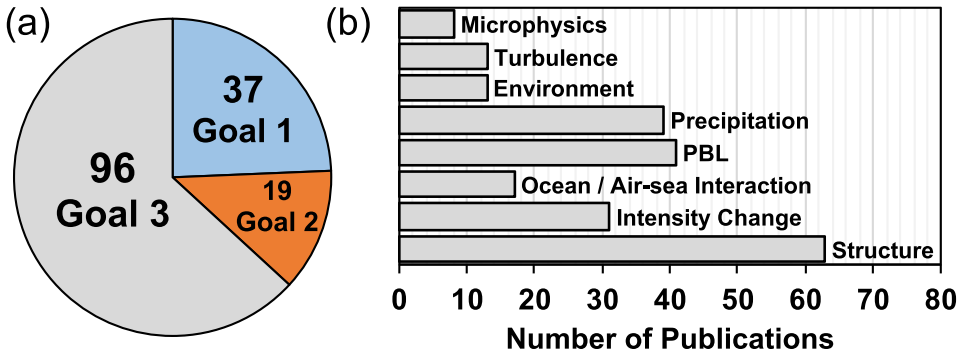

Fig. SB1. (a) Number of publications (totaling 152) from 2006 to 2020 that include AOML/HRD and affiliated scientists, separated for IFEX goals 1 (24%; "model initialization/evaluation"), 2 (13%; "real-time monitoring"), and 3 (63%; "physical processes"); and (b) the total number of publications within goal 3 that are published on various aspects of TC processes [note that many publications have been counted in multiple categories, and therefore, the total in (b) will not add up to 96].

allowed IFEX to benefit through piggybacking research on operationally tasked flights. Many scientists both within and outside of NOAA—too many to fairly convey here—have played integral roles in the development, execution, and success of IFEX. Several funding sources have provided support to this project: NOAA base funds (AOC base funds for flight hours and AOML base funds for HRD manpower and travel), CIMAS, NOAA's Joint Hurricane Testbed (JHT), HFIP (for flight hours, expendables, and travel), and the 2018 and 2019 Hurricane Supplementals (for flight hours and expendables). We thank Michael Brennan (NHC), Ricardo Domingues (UM/CIMAS, AOML/PhOD), Ed Zipser, Jeff Halverson, and an anonymous reviewer for their helpful comments that improved this manuscript.

Data availability statement. AOML/HRD collects and maintains quality-controlled, research-quality NOAA P-3 and G-IV aircraft data for the hurricane field program, in partnership with OMAO/AOC, and makes those data available on its webpage: www.aoml.noaa.gov/data-products/#hurricanedata. AOML/HRD also provides real-time products and model fields from operational and experimental forecast models (e.g., HWRF, basin-scale HWRF, and HAFS), which are available at https://storm.aoml.noaa.gov/. AOML/HRD is committed to facilitate full and open access to data in a timely manner during and after the annual hurricane field program.

References

Abarca, S. F., M. T. Montgomery, S. A. Braun, and J. Dunion, 2016: On the secondary eyewall formation of Hurricane Edouard (2014). *Mon. Wea. Rev.*, **144**, 3321–3331, https://doi.org/10.1175/MWR-D-15-0421.1.

Aberson, S. D., 2003: Targeted observations to improve operational tropical cyclone track forecast guidance. *Mon. Wea. Rev.*, **131**, 1613–1628, https://doi.org/10.1175//2550.1.

——, 2010: 10 years of hurricane synoptic surveillance (1997–2006). *Mon. Wea. Rev.*, **138**, 1536–1549, https://doi.org/10.1175/2009MWR3090.1.

——, A. Aksoy, K. J. Sellwood, T. Vukicevic, and X. Zhang, 2015: Assimilation of high-resolution tropical cyclone observations with an ensemble Kalman filter using HEDAS: Evaluation of 2008–11 HWRF forecasts. *Mon. Wea. Rev.*, **143**, 511–523, https://doi.org/10.1175/MWR-D-14-00138.1.

——, K. J. Sellwood, and P. A. Leighton, 2017: Calculating dropwindsonde location and time from TEMP-DROP messages for accurate assimilation and analysis. *J. Atmos. Oceanic Technol.*, **34**, 1673–1678, https://doi.org/10.1175/JTECH-D-17-0023.1.

Ahern, K., M. A. Bourassa, R. E. Hart, J. A. Zhang, and R. F. Rogers, 2019: Observed kinematic and thermodynamic structure in the hurricane boundary layer during intensity change. *Mon. Wea. Rev.*, **147**, 2765–2785, https://doi.org/10.1175/MWR-D-18-0380.1.

Aksoy, A., 2013: Storm-relative observations in tropical cyclone data assimilation with an ensemble Kalman filter. *Mon. Wea. Rev.*, **41**, 506–522, https://doi.org/10.1175/MWR-D-12-00094.1.

——, S. Lorsolo, T. Vukicevic, K. J. Sellwood, S. D. Aberson, and F. Zhang, 2012: The HWRF Hurricane Ensemble Data Assimilation System (HEDAS) for high-resolution data: The impact of airborne Doppler radar observations in an OSSE. *Mon. Wea. Rev.*, **140**, 1843–1862, https://doi.org/10.1175/MWR-D-11-00212.1.

——, S. D. Aberson, T. Vukicevic, K. J. Sellwood, and X. Zhang, 2013: Assimilation of high-resolution tropical cyclone observations with an ensemble Kalman filter using NOAA/AOML/HRD's HEDAS: Evaluation of the 2008–11 vortex-scale analyses. *Mon. Wea. Rev.*, **143**, 511–523, https://doi.org/10.1175/MWR-D-12-00194.1.

Alaka, G. J., Jr., X. Zhang, S. G. Gopalakrishnan, S. B. Goldenberg, and F. D. Marks, 2017: Performance of basin-scale HWRF tropical cyclone track forecasts. *Wea. Forecasting*, **32**, 1253–1271, https://doi.org/10.1175/WAF-D-16-0150.1.

——, ——, ——, Z. Zhang, F. D. Marks Jr., and R. Atlas, 2019: Track uncertainty in high-resolution HWRF ensemble forecasts of Hurricane Joaquin. *Wea. Forecasting*, **34**, 1889–1908, https://doi.org/10.1175/WAF-D-19-0028.1.

Alford, A. A., J. A. Zhang, M. I. Biggerstaff, P. Dodge, F. D. Marks, and D. J. Bodine, 2020: Transition of the hurricane boundary layer during the landfall of Hurricane Irene. *J. Atmos. Sci.*, **77**, 3509–3531, https://doi.org/10.1175/JAS-D-19-0290.1.

Alvey, G. R., III, J. Zawislak, and E. Zipser, 2015: Precipitation properties observed during tropical cyclone intensity change. *Mon. Wea. Rev.*, **143**, 4476–4492, https://doi.org/10.1175/MWR-D-15-0065.1.

——, E. Zipser, and J. Zawislak, 2020: How does Hurricane Edouard (2014) evolve toward symmetry before rapid intensification? A high-resolution ensemble study. *J. Atmos. Sci.*, **77**, 1329–1351, https://doi.org/10.1175/JAS-D-18-0355.1.

Avila, L. A., S. R. Stewart, R. Berg, and A. B. Hagen, 2020: National Hurricane Center tropical cyclone report: Hurricane Dorian (AL052019). National Hurricane Center Rep., 74 pp., www.nhc.noaa.gov/data/tcr/AL052019_Dorian.pdf.

Berg, R., 2016: National Hurricane Center tropical cyclone report: Hurricane Joaquin (AL112015). National Hurricane Center Rep., 36 pp., www.nhc.noaa.gov/data/tcr/AL112015_Joaquin.pdf.

——, and B. J. Reinhart, 2021: National Hurricane Center tropical cyclone report: Hurricane Sally (AL192020). National Hurricane Center Rep., 69 pp., www.nhc.noaa.gov/data/tcr/AL192020_Sally.pdf.

Beven, J. L., II, R. Berg, and A. Hagen, 2019: National Hurricane Center tropical cyclone report: Hurricane Michael (AL142018). National Hurricane Center Rep., 86 pp., www.nhc.noaa.gov/data/tcr/AL142018_Michael.pdf.

Bhatia, K. T., and D. S. Nolan, 2013: Relating the skill of tropical cyclone intensity forecasts to the synoptic environment. *Wea. Forecasting*, **28**, 961–980, https://doi.org/10.1175/WAF-D-12-00110.1.

Black, P., L. Harrison, M. Beaubien, R. Bluth, R. Woods, A. Penny, R. W. Smith, and J. D. Doyle, 2017: High-Definition Sounding System (HDSS) for atmospheric profiling. *J. Atmos. Oceanic Tech.*, **34**, 777–796, https://doi.org/10.1175/JTECH-D-14-00210.1.

Blake, E. S., and D. A. Zelinsky, 2018: National Hurricane Center tropical cyclone report: Hurricane Harvey (AL092017). National Hurricane Center Rep., 77 pp., www.nhc.noaa.gov/data/tcr/AL092017_Harvey.pdf.

Braun, S. A., P. A. Newman, and G. M. Heymsfield, 2016: NASA's Hurricane and Severe Storm Sentinel (HS3) investigation. *Bull. Amer. Meteor. Soc.*, **97**, 2085–2102, https://doi.org/10.1175/BAMS-D-15-00186.1.

Bu, Y. P., R. G. Fovell, and K. L. Corbosiero, 2017: The influences of boundary layer mixing and cloud-radiative forcing on tropical cyclone size. *J. Atmos. Sci.*, **74**, 1273–1292, https://doi.org/10.1175/JAS-D-16-0231.1.

Bucci, L. R., C. O'Handley, G. D. Emmitt, J. A. Zhang, K. Ryan, and R. Atlas, 2018: Validation of an airborne Doppler wind lidar in tropical cyclones. *Sensors*, **18**, 4288, https://doi.org/10.3390/s18124288.

Cangialosi, J. P., A. S. Latto, and R. Berg, 2018: National Hurricane Center tropical cyclone report: Hurricane Irma (AL112017). National Hurricane Center Rep., 111 pp., www.nhc.noaa.gov/data/tcr/AL112017_Irma.pdf.

——, E. Blake, M. DeMaria, A. Penny, A. Latto, E. Rappaport, and V. Tallapragada, 2020: Recent progress in tropical cyclone intensity forecasting at the National Hurricane Center. *Wea. Forecasting*, **35**, 1913–1922, https://doi.org/10.1175/WAF-D-20-0059.1.

Chen, H., and S. Gopalakrishnan, 2015: A study on the asymmetric rapid intensification of Hurricane Early (2010) using the HWRF system. *J. Atmos. Sci.*, **72**, 531–550, https://doi.org/10.1175/JAS-D-14-0097.1.

Christophersen, H., A. Aksoy, J. Dunion, and K. Sellwood, 2017: The impact of NASA Global Hawk unmanned aircraft dropwindsonde observations on tropical cyclone track, intensity, and structure: Case studies. *Mon. Wea. Rev.*, **145**, 1817–1830, https://doi.org/10.1175/MWR-D-16-0332.1.

——, R. Atlas, A. Aksoy, and J. Dunion, 2018: Combined use of satellite observations and Global Hawk unmanned aircraft dropwindsondes for improved tropical cyclone analyses and forecasts. *Wea. Forecasting*, **33**, 1021–1031, https://doi.org/10.1175/WAF-D-17-0167.1.

Cione, J. J., E. A. Kalina, J. A. Zhang, and E. W. Uhlhorn, 2013: Observations of air–sea interaction and intensity change in hurricanes. *Mon. Wea. Rev.*, **141**, 2368–2382, https://doi.org/10.1175/MWR-D-12-00070.1.

——, ——, E. W. Uhlhorn, A. M. Farber, and B. Damiano, 2016: Coyote unmanned aircraft system observations in Hurricane Edouard (2014). *Earth Space Sci.*, **3**, 370–380, https://doi.org/10.1002/2016EA000187.

——, and Coauthors, 2020: Eye of the storm: Observing hurricanes with a small unmanned aircraft system. *Bull. Amer. Meteor. Soc.*, **101**, E186–E205, https://doi.org/10.1175/BAMS-D-19-0169.1.

Didlake, A. C., G. H. Heymsfield, P. D. Reasor, and S. R. Guimond, 2017: Concentric eyewall asymmetries in Gonzalo (2014) observed by airborne radar. *Mon. Wea. Rev.*, **145**, 729–749, https://doi.org/10.1175/MWR-D-16-0175.1.

——, P. D. Reasor, R. F. Rogers, and W.-C. Lee, 2018: Dynamics of the transition from spiral rainbands to a secondary eyewall in Hurricane Earl (2010). *J. Atmos. Sci.*, **75**, 2909–2929, https://doi.org/10.1175/JAS-D-17-0348.1.

Domingues, R., and Coauthors, 2019: Ocean observations in support of studies and forecasts of tropical and extratropical cyclones. *Front. Mar. Sci.*, **6**, 23, https://doi.org/10.3389/fmars.2019.00446.

Dong, J., and Coauthors, 2017: Impact of assimilating underwater glider data on Hurricane Gonzalo (2014) forecasts. *Wea. Forecasting*, **32**, 1143–1159, https://doi.org/10.1175/WAF-D-16-0182.1.

——, and Coauthors, 2020: The evaluation of real-time Hurricane Analysis and Forecast System (HAFS) Stand-Alone Regional (SAR) model performance for the 2019 Atlantic hurricane season. *Atmosphere*, **11**, 16, https://doi.org/10.3390/atmos11060617.

Dougherty, E. M., J. Molinari, R. F. Rogers, J. A. Zhang, and J. P. Kossin, 2018: Hurricane Bonnie (1998): Maintaining intensity during high vertical wind shear and an eyewall replacement cycle. *Mon. Wea. Rev.*, **146**, 3383–3399, https://doi.org/10.1175/MWR-D-18-0030.1.

Doyle, J. D., and Coauthors, 2017: A view of tropical cyclones from above: The Tropical Cyclone Intensity (TCI) experiment. *Bull. Amer. Meteor. Soc.*, **98**, 2113–2134, https://doi.org/10.1175/BAMS-D-16-0055.1.

Emanuel, K. A., 1995: Sensitivity of tropical cyclones to surface exchange coefficients and a revised steady-state model incorporating eye dynamics. *J. Atmos. Sci.*, **52**, 3969–3976, https://doi.org/10.1175/1520-0469(1995)052<3969:SOTCTS>2.0.CO;2.

Fernandez, D. E., E. M. Kerr, A. Castells, J. R. Carswell, S. J. Frasier, P. S. Chang, P. G. Black, and F. D. Marks, 2005: IWRAP: The Imaging Wind and Rain Airborne Profiler for remote sensing of the ocean and the atmospheric boundary layer within tropical cyclones. *IEEE Trans. Geosci. Remote Sens.*, **43**, 1775–1787, https://doi.org/10.1109/TGRS.2005.851640.

Fischer, M. S., R. F. Rogers, and P. D. Reasor, 2020: The rapid intensification and eyewall replacement cycles of Hurricane Irma (2017). *Mon. Wea. Rev.*, **148**, 981–1004, https://doi.org/10.1175/MWR-D-19-0185.1.

Fuchs-Stone, Z., D. J. Raymond, and S. Stenic, 2020: OTREC2019: Convection over the east Pacific and southwest Caribbean. *Geophys. Res. Lett.*, **47**, e2020GL087564, https://doi.org/10.1029/2020GL087564.

Gall, R., J. Franklin, F. Marks, E. N. Rappaport, and F. Toepfer, 2013: The Hurricane Forecast Improvement Project. *Bull. Amer. Meteor. Soc.*, **94**, 329–343, https://doi.org/10.1175/BAMS-D-12-00071.1.

Gamache, J. F., 1997: Evaluation of a fully three-dimensional variational Doppler analysis technique. Preprints, *28th Conf. on Radar Meteorology*, Austin, TX, Amer. Meteor. Soc., 422–423.

Goerss, J. S., 2009: Impact of satellite observations on the tropical cyclone track forecasts of the Navy Operational Global Atmospheric Prediction System. *Mon. Wea. Rev.*, **137**, 41–50, https://doi.org/10.1175/2008MWR2601.1.

Gopalakrishnan, S. G., F. Marks Jr., J. A. Zhang, X. Zhang, J.-W. Bao, and V. Tallapragada, 2013: A study of the impacts of vertical diffusion on the structure and intensity of the tropical cyclones using the high-resolution HWRF system. *J. Atmos. Sci.*, **70**, 524–541, https://doi.org/10.1175/JAS-D-11-0340.1.

——, and Coauthors, 2020: 2019 Hurricane Forecast Improvement Project R&D activities summary: Recent results and operational implementation. HFIP Tech. Rep. HFIP2020-1, 45 pp., https://doi.org/10.25923/qzd3-m787.

Guimond, S. R., L. Tian, G. M. Heymsfield, and S. J. Frasier, 2014: Wind retrieval algorithms for the IWRAP and HIWRAP airborne doppler radars with applications to hurricanes. *J. Atmos. Oceanic Technol.*, **31**, 1189–1215, https://doi.org/10.1175/JTECH-D-13-00140.1.

——, P. D. Reasor, G. M. Heymsfield, and M. M. McLinden, 2020: The dynamics of vortex Rossby waves and secondary eyewall development in Hurricane Matthew (2016): New insights from radar measurements. *J. Atmos. Sci.*, **77**, 2349–2374, https://doi.org/10.1175/JAS-D-19-0284.1.

Hazelton, A. T., L. Harris, and S.-J. Lin, 2018: Evaluation of tropical cyclone structure forecasts in a high-resolution version of the multiscale GFDL fvGFS model. *Wea. Forecasting*, **33**, 419–442, https://doi.org/10.1175/WAF-D-17-0140.1.

——, X. Zhang, W. Ramstrom, S. Gopalakrishan, F. D. Marks, and J. A. Zhang, 2020: High-resolution ensemble HFV3 forecasts of Hurricane Michael (2018): Rapid intensification in shear. *Mon. Wea. Rev.*, **148**, 2009–2032, https://doi.org/10.1175/MWR-D-19-0275.1.

Holbach, H. M., E. W. Uhlhorn, and M. A. Bourassa, 2018: Off-nadir SFMR brightness temperature measurements in high-wind conditions. *J. Atmos. Oceanic Technol.*, **35**, 1865–1879, https://doi.org/10.1175/JTECH-D-18-0005.1.

Jaimes, B., L. K. Shay, and E. W. Uhlhorn, 2015: Enthalpy and momentum fluxes during Hurricane Earl relative to underlying ocean features. *Mon. Wea. Rev.*, **43**, 111–131, https://doi.org/10.1175/MWR-D-13-00277.1.

Kaplan, J., and M. DeMaria, 2003: Large-scale characteristics of rapidly intensifying tropical cyclones in the North Atlantic basin. *Wea. Forecasting*, **18**, 1093–1108, https://doi.org/10.1175/1520-0434(2003)018<1093:LCORIT>2.0.CO;2.

——, and Coauthors, 2015: Evaluating environmental impacts on tropical cyclone rapid intensification predictability utilizing statistical models. *Wea. Forecasting*, **30**, 1374–1396, https://doi.org/10.1175/WAF-D-15-0032.1.

Klotz, B. W., and E. W. Uhlhorn, 2014: Improved stepped frequency microwave radiometer tropical cyclone surface winds in heavy precipitation. *J. Atmos. Oceanic Technol.*, **31**, 2392–2408, https://doi.org/10.1175/JTECH-D-14-00028.1.

Latto, A., and R. Berg, 2020: National Hurricane Center tropical cyclone report: Tropical Storm Imelda (AL112019). National Hurricane Center Rep., 28 pp., www.nhc.noaa.gov/data/tcr/AL112019_Imelda.pdf.

——, A. Hagen, and R. Berg, 2021: National Hurricane Center tropical cyclone report: Hurricane Isaias (AL092020). National Hurricane Center Rep., 84 pp., www.nhc.noaa.gov/data/tcr/AL092020_Isaias.pdf.

Leighton, H., S. Gopalakrishnan, J. A. Zhang, R. F. Rogers, Z. Zhang, and V. Tallapragada, 2018: Azimuthal distribution of deep convection, environmental factors, and tropical cyclone rapid intensification: A perspective from HWRF ensemble forecasts of Hurricane Edouard (2014). *J. Atmos. Sci.*, **75**, 275–295, https://doi.org/10.1175/JAS-D-17-0171.1.

——, R. Black, X. Zhang, F. D. Marks, and S. G. Gopalakrishnan, 2020: Ice particle size distributions from composites of microphysics observations collected in tropical cyclones. *Geophys. Res. Lett.*, **47**, e2020GL088762, https://doi.org/10.1029/2020GL088762.

Lu, X., X. Wang, M. Tong, and V. Tallapragada, 2017: GSI-based, continuously cycled, dual-resolution hybrid ensemble–variational data assimilation System for HWRF: System description and experiments with Edouard (2014). *Mon. Wea. Rev.*, **145**, 4877–4898, https://doi.org/10.1175/MWR-D-17-0068.1.

Magnusson, L., and Coauthors, 2019: ECMWF activities for improved hurricane forecasts. *Bull. Amer. Meteor. Soc.*, **100**, 445–458, https://doi.org/10.1175/BAMS-D-18-0044.1.

Marks, F., and Coauthors, 2019: Hurricane forecast improvement program five-year plan: 2019-2024. Proposed framework for addressing Section 104 of the Weather Research Forecasting Innovation Act of 2017. National Oceanic and Atmospheric Administration Strategic Plan, 83 pp., www.hfip.org/documents/HFIP_Strategic_Plan_20190625.pdf.

Martinez, J., M. M. Bell, J. L. Vigh, and R. F. Rogers, 2017: Examining tropical cyclone structure and intensification with the FLIGHT+ dataset from 1999 to 2012. *Mon. Wea. Rev.*, **145**, 4401–4421, https://doi.org/10.1175/MWR-D-17-0011.1.

——, ——, R. F. Rogers, and J. D. Doyle, 2019: Axisymmetric potential vorticity evolution of Hurricane Patricia (2015). *J. Atmos. Sci.*, **76**, 2043–2063, https://doi.org/10.1175/JAS-D-18-0373.1.

Ming, J., and J. A. Zhang, 2016: Effects of surface flux parameterization on the numerically simulated intensity and structure of Typhoon Morakot (2009). *Adv. Atmos. Sci.*, **33**, 58–72, https://doi.org/10.1007/s00376-015-4202-z.

Molinari, J., J. Frank, and D. Vollaro, 2013: Convective bursts, downdraft cooling, and boundary layer recovery in a sheared tropical storm. *Mon. Wea. Rev.*, **141**, 1048–1060, https://doi.org/10.1175/MWR-D-12-00135.1.

——, J. A. Zhang, R. F. Rogers, and D. Vollaro, 2019: Repeated eyewall replacement cycles in Hurricane Frances (2004). *Mon. Wea. Rev.*, **147**, 2009–2022, https://doi.org/10.1175/MWR-D-18-0345.1.

Montgomery, M. T., J. A. Zhang, and R. K. Smith, 2014: An analysis of the observed low-level structure of rapidly intensifying and mature Hurricane Earl (2010). *Quart. J. Roy. Meteor. Soc.*, **140**, 2132–2146, https://doi.org/10.1002/qj.2283.

NCEI, 2020: Billion-dollar weather and climate disasters: Overview. NOAA, www.ncdc.noaa.gov/billions/.

Nguyen, L. T., R. F. Rogers, and P. D. Reasor, 2017: Thermodynamic and kinematic influences on precipitation symmetry in sheared tropical cyclones: Bertha and Cristobal (2014). *Mon. Wea. Rev.*, **145**, 4423–4446, https://doi.org/10.1175/MWR-D-17-0073.1.

——, ——, J. A. Zawislak, and J. A. Zhang, 2019: Assessing the influence of convective downdrafts and surface enthalpy fluxes on tropical cyclone intensity change in moderate vertical wind shear. *Mon. Wea. Rev.*, **147**, 3519–3534, https://doi.org/10.1175/MWR-D-18-0461.1.

Pasch, R. J., A. B. Penny, and R. Berg, 2019: National Hurricane Center tropical cyclone report: Hurricane Maria (AL152017). National Hurricane Center Rep., 48 pp., www.nhc.noaa.gov/data/tcr/AL112017_Irma.pdf.

——, R. Berg, D. P. Roberts, and P. P. Papin, 2021: National Hurricane Center tropical cyclone report: Hurricane Laura (AL132020). National Hurricane Center Rep., 75 pp., www.nhc.noaa.gov/data/tcr/AL132020_Laura.pdf.

PopStefanija, I., C. W. Fairall, and E. J. Walsh, 2021: Mapping of directional ocean wave spectra in hurricanes and other environments. *IEEE Trans. Geosci. Remote Sens*., **59**, 9007–9020, https://doi.org/10.1109/TGRS.2020.3042904.

Pu, Z., S. Zhang, M. Tong, and V. Tallapragada, 2016: Influence of the self-consistent regional ensemble background error covariance on hurricane inner-core data assimilation with the GSI-based hybrid system for HWRF. *J. Atmos. Sci.*, **73**, 4911–4925, https://doi.org/10.1175/JAS-D-16-0017.1.

Rappaport, E. N., 2000: Loss of life in the United States associated with recent Atlantic tropical cyclones. *Bull. Amer. Meteor. Soc.*, **81**, 2065–2073, https://doi.org/10.1175/1520-0477(2000)081<2065:LOLITU>2.3.CO;2.

Reasor, P. D., M. D. Eastin, and J. F. Gamache, 2009: Rapidly intensifying Hurricane Guillermo (1997). Part I: Low-wavenumber structure and evolution. *Mon. Wea. Rev.*, **137**, 603–631, https://doi.org/10.1175/2008MWR2487.1.

——, R. F. Rogers, and S. Lorsolo, 2013: Environmental flow impacts on tropical cyclone structure diagnosed from airborne Doppler radar composites. *Mon. Wea. Rev.*, **141**, 2949–2969, https://doi.org/10.1175/MWR-D-12-00334.1.

Rios-Berrios, R., C. A. Davis, and R. D. Torn, 2018: A hypothesis for the intensification of tropical cyclones under moderate vertical wind shear. *J. Atmos. Sci.*, **75**, 4149–4173, https://doi.org/10.1175/JAS-D-18-0070.1.

Rogers, R. F., and Coauthors, 2006: The Intensity Forecasting Experiment (IFEX): A NOAA multiyear field program for improving tropical cyclone intensity forecasts. *Bull. Amer. Meteor. Soc.*, **87**, 1523–1537, https://doi.org/10.1175/BAMS-87-11-1523.

——, and Coauthors, 2013a: NOAA's Hurricane Intensity Forecasting Experiment: A progress report. *Bull. Amer. Meteor. Soc.*, **94**, 859–882, https://doi.org/10.1175/BAMS-D-12-00089.1.

——, P. D. Reasor, and S. Lorsolo, 2013b: Airborne Doppler observations of the inner-core structural differences between intensifying and steady-state tropical cyclones. *Mon. Wea. Rev.*, **141**, 2970–2991, https://doi.org/10.1175/MWR-D-12-00357.1.

——, ——, and J. Zhang, 2015: Multiscale structure and evolution of Hurricane Earl (2010) during rapid intensification. *Mon. Wea. Rev.*, **143**, 536–562, https://doi.org/10.1175/MWR-D-14-00175.1.

——, J. Zhang, J. Zawislak, H. Jiang, G. R. Alvey, III, E. J. Zipser, and S. N. Stevenson, 2016: Observations of the structure and evolution of Hurricane Edouard (2014) during intensity change. Part II: Kinematic structure and the distribution of deep convection. *Mon. Wea. Rev.*, **144**, 3355–3376, https://doi.org/10.1175/MWR-D-16-0017.1.

——, and Coauthors, 2017: Rewriting the tropical record books: The extraordinary intensification of Hurricane Patricia (2015). *Bull. Amer. Meteor. Soc.*, **98**, 2091–2112, https://doi.org/10.1175/BAMS-D-16-0039.1.

——, C. S. Velden, J. A. Zawislak, and J. A. Zhang, 2019: Tropical cyclones and hurricanes: Observations. *Reference Module in Earth Systems and Environmental Sciences*, Elsevier. 25 pp.

——, P. D. Reasor, J. A. Zawislak, and L. T. Nguyen, 2020: Precipitation processes and vortex alignment during the intensification of a weak tropical cyclone in moderate vertical shear. *Mon. Wea. Rev.*, **148**, 1899–1929, https://doi.org/10.1175/MWR-D-19-0315.1.

Ryan, K., L. Bucci, J. Delgado, R. Atlas, and S. Murillo, 2018: Impact of Gulfstream-IV dropsondes on tropical cyclone prediction in a regional OSSE system. *Mon. Wea. Rev.*, **147**, 2961–2977, https://doi.org/10.1175/MWR-D-18-0157.1.

Sellwood, K. J., J. A. Sippel, and A. Aksoy, 2020: Optimizing dropsonde levels for data assimilation. *20th Symp. on Meteorological Observation and Instrumentation*, Boston, MA, Amer. Meteor. Soc., 5.6, https://ams.confex.com/ams/2020Annual/meetingapp.cgi/Paper/365847.

Shay, L. K., G. J. Goni, and P. G. Black, 2000: Effects of a warm oceanic feature on Hurricane Opal. *Mon. Wea. Rev.*, **128**, 1366–1383, https://doi.org/10.1175/1520-0493(2000)128<1366:EOAWOF>2.0.CO;2.

Smith, R. K., J. A. Zhang, and M. T. Montgomery, 2017: The dynamics of intensification in an HWRF simulation of Hurricane Earl (2010). *Quart. J. Roy. Meteor. Soc.*, **143**, 297–308, https://doi.org/10.1002/qj.2922.

Steward, J. L., A. Aksoy, and Z. S. Haddad, 2017: Parallel direct solution of the ensemble square root Kalman filter equations with observation principal components. *J. Atmos. Oceanic Technol.*, **34**, 1867–1884, https://doi.org/10.1175/JTECH-D-16-0140.1.

——, J. E. Roman, A. L. Daviña, and A. Aksoy, 2018: Parallel direct solution of the covariance-localized ensemble square root Kalman filter equations with matrix functions. *Mon. Wea. Rev.*, **146**, 2819–2836, https://doi.org/10.1175/MWR-D-18-0022.1.

Stewart, S. R., 2017: National Hurricane Center tropical cyclone report: Hurricane Matthew (AL142016). National Hurricane Center Rep., 96 pp., www.nhc.noaa.gov/data/tcr/AL142016_Matthew.pdf.

——, and R. Berg, 2019: National Hurricane Center tropical cyclone report: Hurricane Florence (AL062018). National Hurricane Center Rep., 98 pp., www.nhc.noaa.gov/data/tcr/AL062018_Florence.pdf.

Sumwalt, R. L., III, C. A. Hart, E. F. Weener, and T. B. Dinh-Zahr, 2017: Safety recommendation report: Tropical cyclone information for mariners. National Transportation Safety Board Tech. Rep. MSR-17/02, 21 pp., www.ntsb.gov/investigations/AccidentReports/Reports/MSR1702.pdf.

Susca-Lopata, G., J. Zawislak, E. J. Zipser, and R. F. Rogers, 2015: The role of observed environmental conditions and precipitation evolution in the rapid intensification of Hurricane Earl (2010). *Mon. Wea. Rev.*, **143**, 2207–2223, https://doi.org/10.1175/MWR-D-14-00283.1.

Taylor, A., and B. Glahn, 2008: Probabilistic guidance for hurricane storm surge. *19th Conf. on Probability and Statistics*, New Orleans, LA, Amer. Meteor. Soc., 7.4., https://ams.confex.com/ams/pdfpapers/132793.pdf.

Tong, M., V. Tallapragada, E. Liu, B. Zhang, W. Wang, C. Kieu, and S. Liu, 2014: Assimilation of aircraft reconnaissance observations with HWRF hybrid data assimilation system. *31st Conf. on Hurricanes and Tropical Meteorology*, San Diego, CA, Amer. Meteor. Soc., 14D.4, https://ams.confex.com/ams/31Hurr/webprogram/Paper245188.html.

——, and Coauthors, 2018: Impact of assimilating aircraft reconnaissance observations on tropical cyclone initialization and prediction using operational HWRF and GSI ensemble-variational hybrid data assimilation. *Mon. Wea. Rev.*, **146**, 4155–4177, https://doi.org/10.1175/MWR-D-17-0380.1.

Wadler, J. B., R. F. Rogers, and P. D. Reasor, 2018a: The relationship between spatial variations in the structure of convective bursts and tropical cyclone intensification as determined by airborne Doppler radar. *Mon. Wea. Rev.*, **146**, 761–780, https://doi.org/10.1175/MWR-D-17-0213.1.

——, J. A. Zhang, B. Jaimes, and L. K. Shay, 2018b: Downdrafts and the evolution of boundary layer thermodynamics in Hurricane Earl (2010) before and during rapid intensification. *Mon. Wea. Rev.*, **46**, 3545–3565, https://doi.org/10.1175/MWR-D-18-0090.1.

——, ——, R. F. Rogers, B. Jaimes, and L. K. Shay, 2020: The rapid intensification of Hurricane Michael (2018): Storm structure and the relationship to environmental and air–sea interactions. *Mon. Wea. Rev.*, **149**, 245–267, https://doi.org/10.1175/MWR-D-20-0145.1.

Wang, W., J. A. Sippel, S. Abarca, L. Zhu, B. Liu, Z. Zhang, A. Mehra, and V. Tallapragada, 2018: Improving NCEP HWRF simulations of surface wind and inflow angle in the eyewall area. *Wea. Forecasting*, **33**, 887–898, https://doi.org/10.1175/WAF-D-17-0115.1.

Weng, Y., and F. Zhang, 2012: Assimilating airborne Doppler radar observations with an ensemble Kalman filter for convection-permitting hurricane initialization and prediction: Katrina (2005). *Mon. Wea. Rev.*, **140**, 841–859, https://doi.org/10.1175/2011MWR3602.1.

——, and ——, 2016: Advances in convection-permitting tropical cyclone analysis and prediction through EnKF assimilation of reconnaissance aircraft observations. *J. Meteor. Soc. Japan*, **94**, 345–358, https://doi.org/10.2151/jmsj.2016-018.

Wick, G. A., and Coauthors, 2020: NOAA's Sensing Hazards with Operational Unmanned Technology (SHOUT) experiment observations and forecast impacts. *Bull. Amer. Meteor. Soc.*, **101**, E968–E097, https://doi.org/10.1175/BAMS-D-18-0257.1.

Winterbottom, H., J. A. Sippel, A. Mehra, B. Zhang, and Z. Zhang, 2018: Recent and planned upgrades to operational HWRF data assimilation. *33rd Conf. on Hurricanes and Tropical Meteorology*, Ponte Vedra Beach, FL, Amer. Meteor. Soc., 3C.5, https://ams.confex.com/ams/33HURRICANE/webprogram/Paper338953.html.

Zawislak, J., H. Jiang, G. R. Alvey, III, E. J. Zipser, R. F. Rogers, J. A. Zhang, and S. N. Stevenson, 2016: Observations of the structure and evolution of Hurricane Edouard (2014) during intensity change. Part I: Relationship between the thermodynamic structure and precipitation. *Mon. Wea. Rev.*, **144**, 3333–3354, https://doi.org/10.1175/MWR-D-16-0018.1.

Zelinsky, D. A., 2019: National Hurricane Center tropical cyclone report: Hurricane Lorenzo (AL132019). National Hurricane Center Rep., 22 pp., www.nhc.noaa.gov/data/tcr/AL132019_Lorenzo.pdf.

Zhang, B., J. A. Sippel, B. Liu, M. Tong, Z. Zhang, V. Tallapragada, and A. Mehra, 2018: Impact of assimilating aircraft reconnaissance observations in operational HWRF on improving hurricane forecast for the 2017 Atlantic high-impact storms. *33rd Conf. on Hurricanes and Tropical Meteorology*, Ponte Vedra Beach, FL, Amer. Meteor. Soc., 6A.3. https://ams.confex.com/ams/33HURRICANE/webprogram/Paper340147.html.

Zhang, F., and D. Tao, 2013: Effects of vertical wind shear on the predictability of tropical cyclones. *J. Atmos. Sci.*, **70**, 975–983, https://doi.org/10.1175/JAS-D-12-0133.1.

——, Y. Weng, J. F. Gamache, and F. D. Marks, 2011: Performance of convection-permitting hurricane initialization and prediction during 2008–2010 with ensemble data assimilation of inner-core airborne Doppler radar observations. *Geophys. Res. Lett.*, **38**, L15810, https://doi.org/10.1029/2011GL048469.

Zhang, J. A., and M. T. Montgomery, 2012: Observational estimates of the horizontal eddy diffusivity and mixing length in the low-level region of intense hurricanes. *J. Atmos. Sci.*, **69**, 1306–1316, https://doi.org/10.1175/JAS-D-11-0180.1.

——, and F. D. Marks, 2015: Effects of horizontal diffusion on tropical cyclone intensity change and structure in idealized three-dimensional numerical simulations. *Mon. Wea. Rev.*, **143**, 3981–3995, https://doi.org/10.1175/MWR-D-14-00341.1.

——, and R. F. Rogers, 2019: Effects of parameterized boundary layer structure on hurricane rapid intensification in shear. *Mon. Wea. Rev.*, **147**, 853–871, https://doi.org/10.1175/MWR-D-18-0010.1.

——, S. G. Gopalakrishnan, F. D. Marks, R. F. Rogers, and V. Tallapragada, 2012: A developmental framework for improving hurricane model physical parameterizations using aircraft observations. *Trop. Cyclone Res. Rev.*, **1**, 419–429, https://doi.org/10.6057/2012TCRR04.01.

——, R. F. Rogers, P. Reasor, E. Uhlhorn, and F. D. Marks Jr., 2013: Asymmetric hurricane boundary layer structure from dropsonde composites in relation to the environmental wind shear. *Mon. Wea. Rev.*, **141**, 3968–3984, https://doi.org/10.1175/MWR-D-12-00335.1.

——, D. S. Nolan, R. F. Rogers, and V. Tallapragada, 2015: Evaluating the impact of improvements in the boundary layer parameterization on hurricane intensity and structure forecasts in HWRF. *Mon. Wea. Rev.*, **143**, 3136–3155, https://doi.org/10.1175/MWR-D-14-00339.1.

——, J. J. Cione, E. A. Kalina, E. W. Uhlhorn, T. Hock, and J. A. Smith, 2017a: Observations of infrared sea surface temperature and air–sea interaction in Hurricane Edouard (2014) using GPS dropsondes. *J. Atmos. Oceanic Technol.*, **34**, 1333–1349, https://doi.org/10.1175/JTECH-D-16-0211.1.

——, R. F. Rogers, and V. Tallapragada, 2017b: Impact of parameterized boundary layer structure on tropical cyclone rapid intensification forecasts in HWRF. *Mon. Wea. Rev.*, **145**, 1413–1426, https://doi.org/10.1175/MWR-D-16-0129.1.

——, F. D. Marks, J. A. Sippel, R. F. Rogers, X. Zhang, S. G. Gopalakrishnan, Z. Zhang, and V. Tallapragada, 2018a: Evaluating the impact of improvement in the horizontal diffusion parameterization on hurricane prediction in the operational Hurricane Weather Research and Forecast (HWRF) Model. *Wea. Forecasting*, **33**, 317–329, https://doi.org/10.1175/WAF-D-17-0097.1.

——, R. Atlas, G. D. Emmitt, L. Bucci, and K. Ryan, 2018b: Airborne Doppler wind lidar observations of the tropical cyclone boundary layer. *Remote Sens.*, **10**, 825, https://doi.org/10.3390/rs10060825.

Zhang, X., S. G. Gopalakrishnan, S. Trahan, T. S. Quirino, Q. Liu, Z. Zhang, G. J. Alaka, and V. Tallapragada, 2016: Representing multiple scales in the Hurricane Weather Research and Forecasting modeling system: Design of multiple sets of movable multilevel nesting and the basin-scale HWRF forecast application. *Wea. Forecasting*, **31**, 2019–2034, https://doi.org/10.1175/WAF-D-16-0087.1.

Zhang, Z., and Coauthors, 2020: The impact of stochastic physics-based hybrid GSI/EnKF data assimilation on hurricane forecasts using EMC operational hurricane modeling system. *Atmosphere*, **11**, 801, https://doi.org/10.3390/atmos11080801.